FINITE ELEMENT ANALYSIS OF ELECTRO-DISCHARGE MACHINING PROCESS

by

P. MADHU

DEPARTMENT OF MECHANICAL ENGINEERING

INDIAN INSTITUTE OF TECHNOLOGY, KANPUR

NOVEMBER, 1988

FINITE ELEMENT ANALYSIS OF ELECTRO-DISCHARGE MACHINING PROCESS

A Thesis Submitted
In Partial Fulfilment of the Requirements
for the Degree of
MASTER OF TECHNOLOGY

by

P. MADHU

to the

DEPARTMENT OF MECHANICAL ENGINEERING
INDIAN INSTITUTE OF TECHNOLOGY, KANPUR
NOVEMBER, 1988

ME-1988-M-MAD-FIN

CERTIFICATE

22/11/88

This is to certify that the work entitled, FINITE ELEMENT ANALYSIS OF ELECTRO-DISCHARGE MACHINING PROCESS by Shri P. Madhu has been carried out under our supervision and has not been submitted elsewhere for a degree.

(V.K. JAIN)
Department of Mechanical Engg.
I.I.T. KANPUR-208016

(T. SUNDARARAJAN)
Department of Mechanical Engg.
I.I.T. KANPUR-208016

November 1988

ACKNOWLEDGEMENT

I express my heartfelt gratitude to Dr. T. Sundararajan and Dr. V.K. Jain. They have always been friendly, co-operative and lenient towards me. Their constant guidance and involvement had made this thesis viable.

I express my gratitude to the SPGC for kindly granting me a two semester leave.

I need hardly mention the company of my close friends in the Institute, who made my stay memorable one.

I would like to personally thank Mr. V.Ch. Venkat Rao, Mr. P. Anand Kishore, Mr. C. Diwakar and Mr. Amar J. Barthakur for helping me with the programming part of my thesis.

I express my appreciation to Mr. H.V.C. Srivastava for his help in typing the thesis.

And lastly, I would like to express my love and appreciation for my wife and son for courageously staying alone at home, during the times I had to be away from them for my thesis work

Madhu
22-11-83
Madhu

CONTENTS

LIST OF FIGURES

LIST OF TABLE

NOMENCLATURE

C_p	Specific heat	J/kg K
h	Heat transfer coefficient	w/m^2K
K	Thermal conductivity	w/mK
P	Power	w
Q	Energy input	w
q	Rate of heat flux	w/m^2
T	Temperature	K
T_f	Fluid temperature for convective boundary conditions.	K
T	Ambient temperature	K
t	Time	sec

Greek Symbols.

α	Thermal diffusivity	M^2/hr
ρ	Mass density	kg/m^3
∇	Vector gradient operator	M^{-1}
θ	A constant which denotes the type of finite difference scheme used.	

Subscripts.

av	average
e	Element index
i	Node index
j	Node index
m	Melting
s	Solid

Superscripts.

.	Derivative with respect to time.

ABSTRACT

A thermal model has been developed for predicting the material removal rate during Electro Discharge Machining (EDM). The transient heat conduction equation for the work piece which accounts for the heat absorption due to melting, has been solved by the finite element method. Gaussian heat distribution of power within a spark has been considered and the periodical updating of the shape of the work piece surface has been performed for the first time, unlike in earlier theoretical works. Computations have been performed for a single spark in the form of a pulse and a multi spark situation with a continuous power input. The effect of different variables on the material removal have been calculated and plotted. The observed results seem to match fairly well with the available experimental results.

CHAPTER-I

INTRODUCTION AND LITERATURE SURVEY

1.1 GENERAL BACKGROUND :

There has been a rapid growth in the development of harder and difficult-to-machine metals and alloys during the last two decades. Conventional machining is uneconomical for such materials and the degree of accuracy and surface finish attainable is poor. Merchant(1960) emphasized the need for the development of newer concepts in the machining of metals in order to meet the challenges posed by modern engineering materials. By utilizing the results of basic and applied research, newer machining processes, often called as unconventional machining methods have been developed.

Electric Discharge Machining (EDM) is the process of removal of material from the electrically conducting materials by electrical discharges between two electrodes i.e., anodic work piece and cathodic tool. The inter-electrode gap is filled with a dielectric medium. The aim of the process is to achieve controlled removal of material from the work piece.

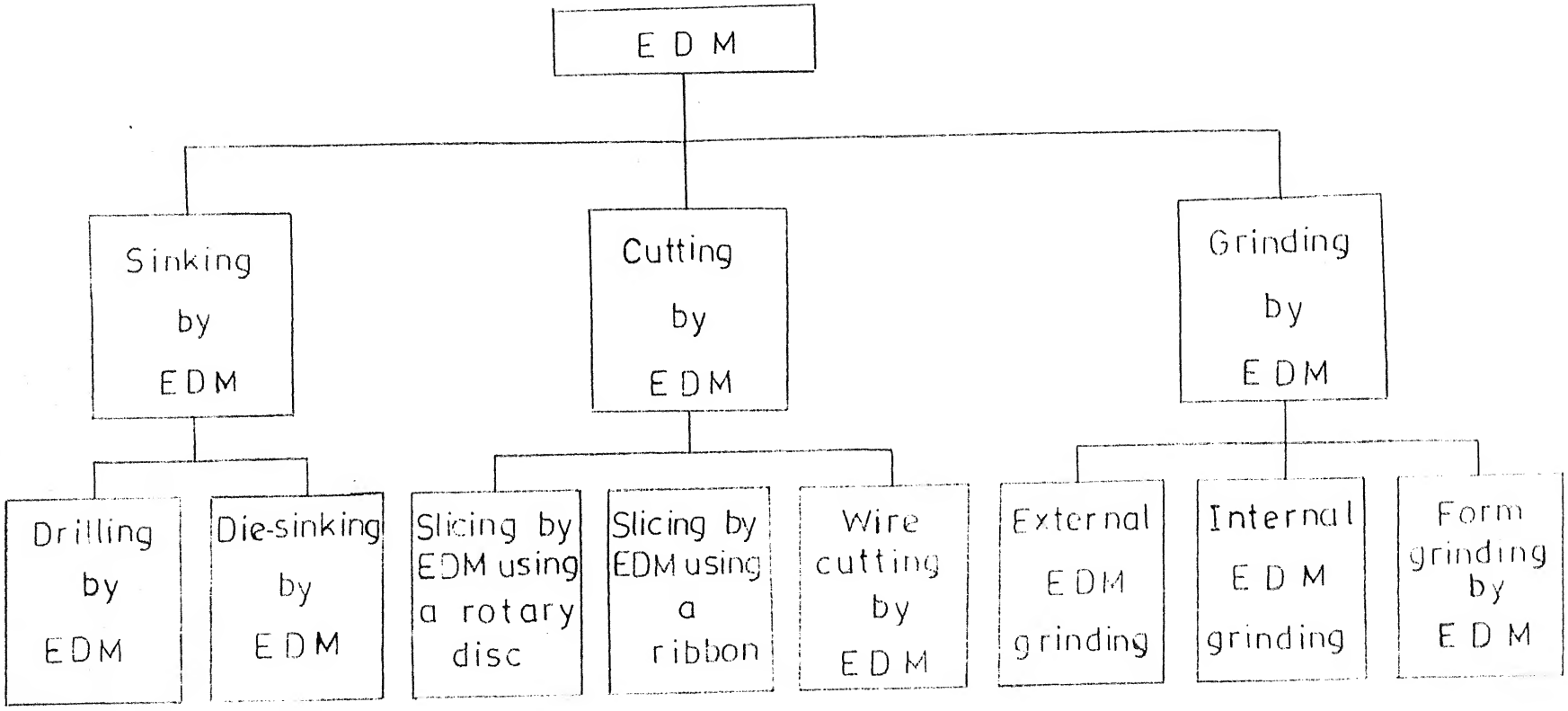

Fig. 1.1 Classification of EDM processes [7]

EDM has found wide applications in the machining of hard metals and alloys which cannot be machined easily by conventional methods. It thus plays a major role in the manufacture of dies, tools etc., made of tungsten carbides, stellites or hard steels. Alloys used in the aeronautical industry,for example, hast alloy, nimonic etc. can be machined conveniently by this process. This process has an added advantage of being capable of machining complicated components from hard materials to a high degree of accuracy and surface finish.

It is important to predict the obtainable work profile from the given machining conditions and specified tool shape. This can be done by knowing the exact mechanism of metal removal and a computational procedure for the same.

The metal removal in EDM is considered to be due to melting and vaporization of anode material. Many attempts [1,2,3,4,5,6] have been made by researchers, to theoretically compute the MRR. But, discrepancy between the analytical and experimental results has been observed as discussed below.

1.2 REVIEW OF PREVIOUS WORK :

Many researchers [1,2,3,4,5,6] have contributed to the study of the EDM process. Most of these researchers considered a single spark in their study and then generalized

the analysis for the whole process. Before proceeding to discuss our own work, we shall briefly present the work done by earlier researchers in this area.

C.C. Marty [1] demonstrated that for a given heat input and a maximum surface temperature , the crater depth and radius of the heat source are correlated by an universal function. His experimental data show that for many materials, the surface temperature is of the same magnitude as the boiling point. Also, the surface temperature in the centre of the spot is practically independent of heat source diameter.

Y. Mukoyama [2] applied the theory of thermal conduction and calculated the relation between the discharge energy, discharge duration, material properties of the electrode and the melting depth at a discharge point. Material removal is considered to be by thermal phenomena and temperature distribution is based on heat conduction equation in cylindrical co-ordinates. The differential equation for temperature distribution is

$$\rho \frac{\partial T}{\partial t} = \alpha\left(\frac{\partial^2 T}{\partial r^2} + \frac{1}{r}\frac{\partial T}{\partial r} + \frac{\partial^2 T}{\partial z^2}\right)$$

The difference between heat supplied and heat taken up due to latent heat of melting is considered to be the actual heat input at the discharge point. It has been observed that crater depth increases with increase in discharge duration upto a certain value and then drops. This is true for all electrode materials. He showed that melting depth is proportional to material removal. Tool wear quantity is attributed to wear. Material removal efficiency is about 5-15 % (15-60 % for graphite tool). The analysis is simplified due to the assumptions like, heat source size is constant regardless of discharge condition and the physical constants of electrodes taken are those at normal conditions.

Jilani and Pandey [3] examined the effect of plasma channel growth on metal removal and found a good correlation between theoretical and experimental results. They proved that in case of steel for a fixed pulse energy, volumetric erosion is not dependent on the current pulse form, but the wear ratio is influenced by the current waveform. They concluded that the theoretical depth to diameter ratio of a crater lies in the range of 3.5 - 34 % and experimental 3-30 % . In order to arrive at these conclusions, they considered a disc shaped heat source and material removal by thermal erosion due to sparking. The governing equation for temperature is

$$T(r,z,t) = \frac{R^2 a^{1/2}}{k\pi^{1/2}} \int_0^1 \frac{dt \exp(-z^2/4at)\exp(-r^2/(4at+R^2))}{t^{1/2}(4at+R^2)}$$

For plasma channel growth, it has been assumed that for a spark, the surface temperature is constant. This model gives comparatively good results for MRR, since plasma channel growth with time and adapted thermal diffusivity (a)* - to account for material removal at boiling point - are taken into consideration. Due to arbitrarily chosen spark diameter, the predicted MRR values are higher than the experimental ones.

Dharmadhikari and Sharma [4] presented a thermal erosion model in which a finite number of heat sources are considered to determine the material removal rate for a single pulse. It has been considered that the heat source which is initially point shaped to be spreading progressively over the crater surface. The energy is assumed to be distributed equally among the sparks and craters formed are hemispherical in shape. Material removal per pulse is given as equal to

$$(8\pi\, \alpha_s^{3/2}\, t_p)\, (\lambda_2^3/Kp)\, P_{av}/J$$

$$MRR = (8\pi\, \alpha_s^{3/2}\, p)\, (\lambda_2^3/K_p) P_{av}/J$$

---

* $a = \frac{k\,1}{\rho\, C^1}$ where $C^1 = C + \frac{M}{T_M}$

where,

$$p = \text{duty factor} = \frac{t_p \text{ (pulse time)}}{t_c \text{ (cycle time)}}$$

$$K_p = 3 P_{av}/2J(t_p)^{0.5}$$

λ_2 = a constant for a given value of K_p.

A Erden and B Kaftanoglu [5] presented two new models. One is based on the uniformly distributed point sources assumption. The other is an approximate, but general model, involving time variation of the heat source and its radius. That is temperature is considered to be a function of heat source density and source radius at a given time. The heat source density and radius are considered to be discrete step functions and based on this continuously variable heat source is simplified to an energy source of constant magnitude.

The governing equation (for constant power) is taken to be

$$T(r,t) = \frac{Q}{2\pi Kr} \text{ erf } C \left[\frac{r}{2(\alpha t)^{1/2}}\right]$$

Out of the many factors affecting the material removal, the authors [5] considered only pulse time power and electrode material. Agreement with the experimental data is shown to be satisfactory for all cases.

R. Snoeys and F. Van Dyck [6] considered melting and vaporization of metal to be dominating the material removal process in EDM. They considered that the portions of the metal where the temperature is larger than or equal to the melting value. Constitute the material which is removed by the EDM process. Their heat transfer model is treated in cylindrical coordinates with no internal heat generation and no mass flow. In order to take into account the latent heat, thermal diffusivity is taken as a function of melting heat, time and temperature the governing equation for temperature distribution is

$$T(r,z,t) = \sum_{n=1}^{\infty} \frac{C_n}{2\lambda_n} J_o(\lambda_n r) \left\{ e^{\lambda_n z} \left[\operatorname{erf}\left(\lambda_n \sqrt{at} + \frac{z}{2\sqrt{at}}\right) - 1 \right] + e^{-\lambda_n z} \left[\operatorname{erf}\left(\lambda_n \sqrt{at} - \frac{z}{2\sqrt{at}}\right) + 1 \right] \right\}$$

where $a = K/C^1$ - adapted thermal diffusivity

Because no vaporization is accounted for, 350 to 500 %. difference is observed between calculated and theoretical upper limit (at 100 %. efficiency).

From above literature survey, it is evident that these models do not account for multi sparks, moving work surfaces (in actual machining, tool and work surfaces are

moving with time), convection of heat to the dielectric and environment, effect of contamination on the dielectric properties etc.

1.3 OBJECTIVES OF PRESENT WORK :

The main objective of the present work is to calculate the material removal rate during electro-Discharge machining.

Till now, researchers have considered the same surface for successive sparks thereby setting a condition that the problem is being repeated for each spark, literally with constant material removal per spark. In the present analysis, the surface is being changed (updated) between every two successive sparks by considering the melting isotherm as the new surface. Due to this, the material removal per spark will vary.

To achieve this objective, the following steps are being proposed.

1. To develop a suitable heat transfer model since the material removal is a thermal process.
2. To apply the finite element analysis for the above problem since numerical methods give fairly good results and also because the geometry of the problem becomes very complicated after partial machining.

3. To find out the amount of material removal for a specified time, applying continuous sparking of known power with Gaussian distribution.

CHAPTER- II

MATHEMATICAL ANALYSIS OF THE PROBLEM

2.1 MECHANISM OF EDM :

Any form of electric discharge is accompanied by some wear of the electrode material. The Electro Discharge Machining (EDM) is based on this spark erosion effect. During EDM, the electric discharge occurs through a gas, liquid or solid, called the dielectric. The necessary condition for a discharge is the ionization of the dielectric by which the molecules of the dielectric are split up into positively charged ions and negatively charged electrons.

The following processes take place when a discharge occurs between the EDM tool (cathode) and the work piece (anode), through a dielectric medium. When a sufficiently high voltage is applied across the electrodes, the intensity of the electric field between them builds up. At some predetermined value of the voltage, the individual electrons break loose from the surface of the cathode and are impelled towards the anode under the influence of electrical field forces. While moving in the inter electrode space, the electrons collide with the neutral molecules of the dielectric,

detaching electrons from them and causing ionization. After some time, the ionization becomes such that a narrow channel of continuous conductivity is formed. Then there is a considerable flow of electrons along the channel to the anode, resulting in a momentary current impulse or discharge. The liberation of a large pulse of energy leads to the generation of high temperature (between 8000° and 12,000°C), causing fusion or partial vaporization of the metal and the dielectric fluid at the point of discharge. The metal, in the form of liquid drops, is dispersed into the space surrounding the electrodes by the explosive pressure of the gaseous products in the discharge. This results in the formation of a tiny crater at the point of discharge in the work piece [7].

Comparatively less metal is eroded from the tool (cathode) than the work piece (anode) due to two reasons.

1. The momentum with which positive ions strike the cathode surface is much less than the momentum with which the electrons-stream impinges on the anode surface.

2. A compressive force is generated on the cathode surface by the spark which helps reduce the tool wear.

A simple EDM set up is shown in Fig. 2.1. Typically the circuit consists of resistor and capacitor elements which draw electrical energy from a DC source. Due to the continuous oscillatory response of the R.C. circuit, the capacitor is charged upto a threshold voltage, at which it discharges electrical energy in the form of a pulse through the circuit. The frequency and shape of the electrical pulse can be adjusted as desired by choosing proper values of resistance and capacitance for the circuit elements. Thus, a short pulse (of the order of micro seconds) of very high energy intensity is generated which results in a spark discharge across the dielectric channel.

2.2 CONSIDERATIONS INVOLVED IN THE THEORETICAL ANALYSIS OF EDM :

The method for calculating the material removal rate due to the impact of an electric pulse, is based upon the assumption that the amount of molten metal right at the end of the an impulse is removed completely. The shock wave generated in the dielectric by the spark, and the rapidly expanding metallic vapour bubble at work surface, aid in clearing up the molten metal. In addition to these phenomenon, the dielectric fluid is often forced to flow through the inter-electrode gap (ieg) for effective material removal. Thus, the amount of molten metal can be determined by the volume limited by the iso-temperature plane of the melting temperature at the end of the pulse and the exposed surface of the electrode metal at the beginning of the spark.

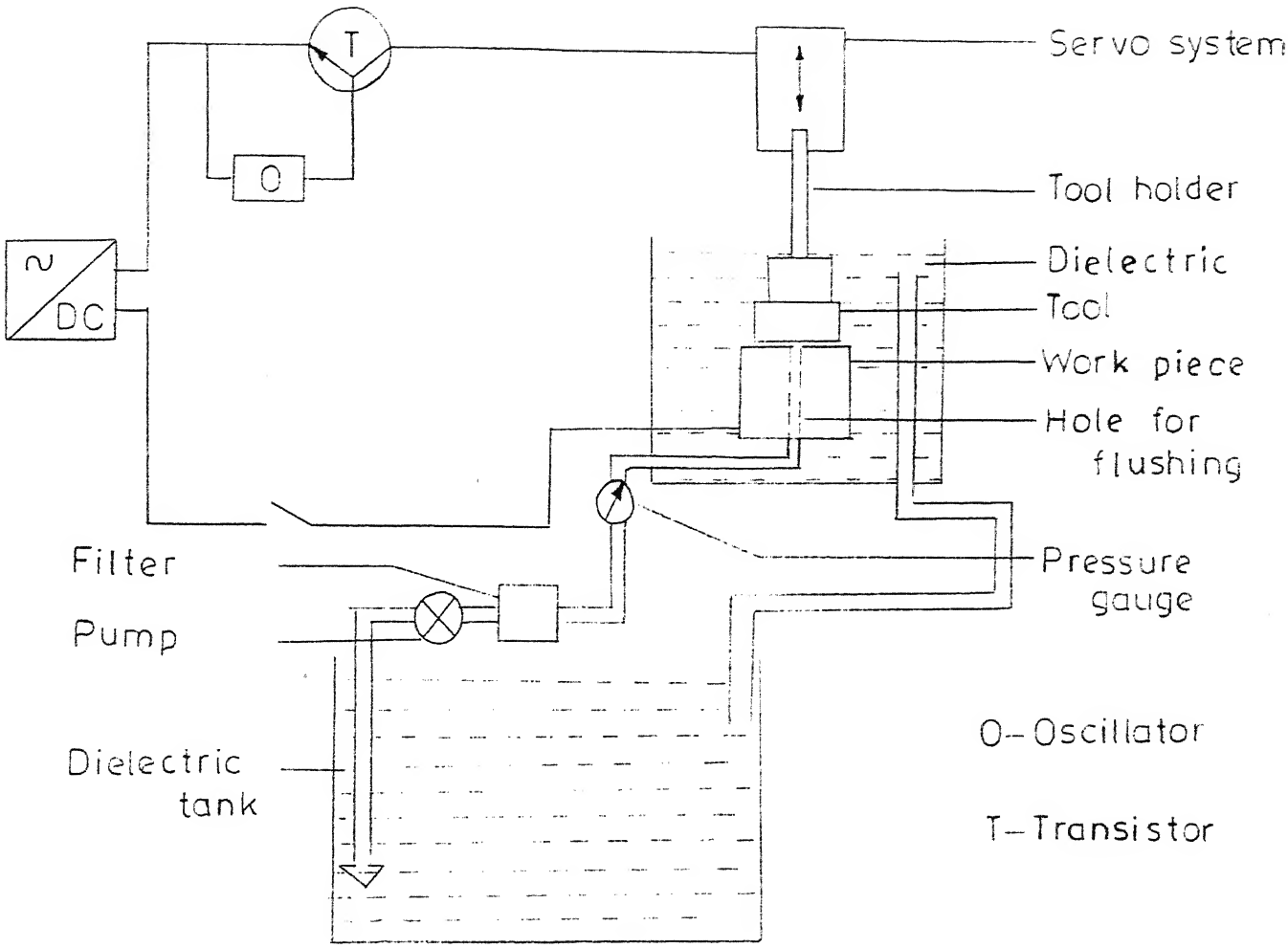

Fig. 2.1 Typical EDM circuit

During a typical electro discharge machining operation, for each electrical pulse, many sparks originate simultaneously from the tool electrode and they strike at the work-surface. Dharmadhikari and Sarma [4] have found that the number of simultaneously produced sparks at any time is of the order of 15. However, it is the function of surface roughness of tool and work. The diameter of the spark itself is of the order 50 microns, while the heat affected area for each individual spark is about a hundred times larger than the spark area [4]. The locations at which the sparks strike on the work-surface and the energy carried by each spark vary randomly and a precise estimation of these quantities is not possible. Also, after partial machining, the surface of the work-piece is filled with many complex-shaped craters. In view of these difficulties the consideration of all the sparks and their interaction with the work-metal is a very difficult proposition for analytical or numerical modelling of the EDM process. Many authors [1,2,3,4,5,6] have considered a single, cylindrical heat source of uniform intensity or many point sources of equal power which are uniformly distributed over the area under the tool electrode. Mathematical analyses have also been performed with assumption that the location of heat source (or heat sources) is at the level of the original unmachined surface.

In the present work, a finite element analysis of the EDM process is performed by considering a given number (N) of sparks to strike at the work-surface. Due to the high pulse frequency, each spark is taken to be a continuous heat source. It is also assumed that the sparks strike at the same locations for all time and each spark is a cylindrical heat source of equal power. The intensity variation within the spark has been assumed to follow a Gaussian distribution. Considering a typical spark which is surrounded by other sparks, it can be taken that only a limited region is affected by the spark. The analysis, therefore, can be simplified by assuming the boundary of the heat affected zone of a particular spark to be loosing no heat to the surrounding zones, while calculating the rate of machining due to a single spark. Approximately, the total machining rate can be calculated by multiplying the individual machining rate by the number of sparks, N.

2.3 HEAT TRANSFER MODEL FOR THE HEAT AFFECTED ZONE OF A SINGLE SPARK :

In the present study each spark is considered to be cylindrical in shape as represented in Fig. 2.2.

Considering the heating due to every spark to be axisymmetric in its neighbourhood, the simplification can be made that there is no temperature variation with respect to the direction θ .

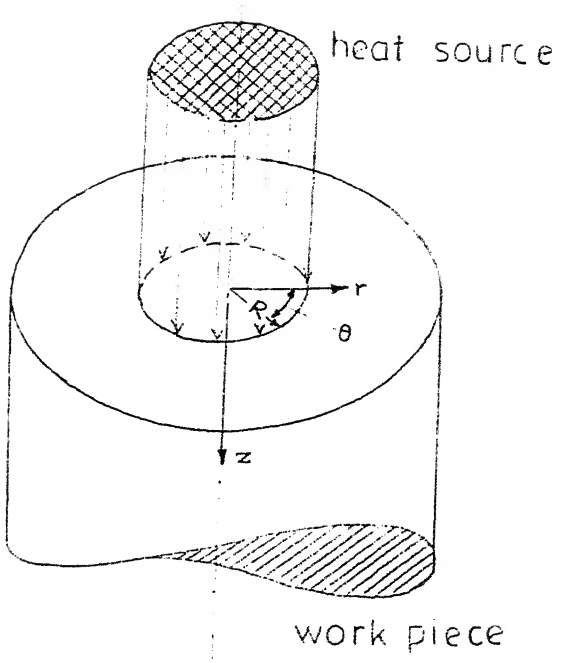

Fig. 2.2 Cylindrical heat source

$$\frac{\partial T}{\partial \theta} = 0 \qquad (2.1)$$

Under the above conditions, the governing heat conduction equation within the work material is given in cylindrical coordinates as

$$\rho C_p \frac{\partial T}{\partial t} = k \left[\frac{\partial}{\partial r} \left(r \frac{\partial T}{\partial r} \right) + \frac{\partial^2 T}{\partial z^2} \right] \qquad (2.2)$$

where, ρ is the density, C_p is the specific heat and k is the thermal conductivity of the work material.

In order to account for the latent heat of melting and evaporation, the specific heat of the electrode material is taken to be a function of temperature as shown in Fig. 2.3. With this the governing equation (2.2) can be written as

$$\rho C_p(T) \frac{\partial T}{\partial t} = k \left[\frac{\partial}{\partial r} \left(r \frac{\partial T}{\partial r} \right) + \frac{\partial^2 T}{\partial z^2} \right] \qquad (2.3)$$

Average values of different properties are used as their variations are not large in the range of temperatures of interest in this problem.

The following boundary and initial conditions are to be satisfied, for the heat affected zone of a single spark, as shown in Fig. 2.4.

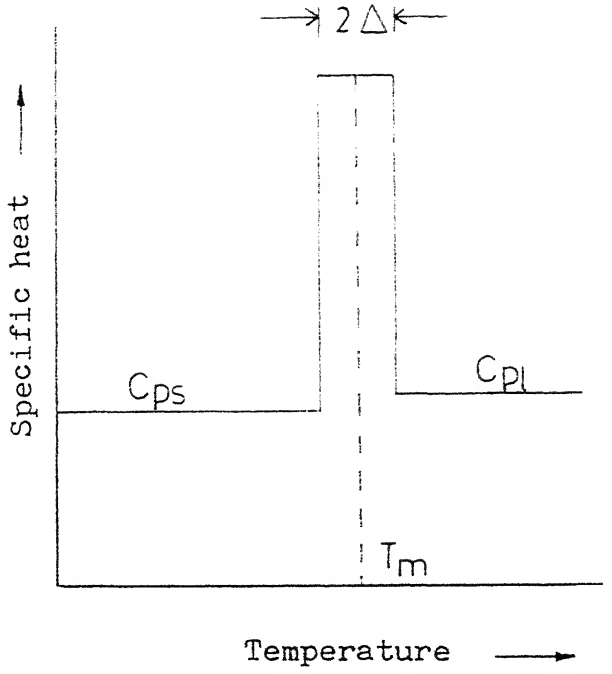

C_{ps} = Specific heat of solid

C_{pl} = Specific heat of liquid

T_m = Melting temperature

Fig. 2.3 Specific heat variation with temperature

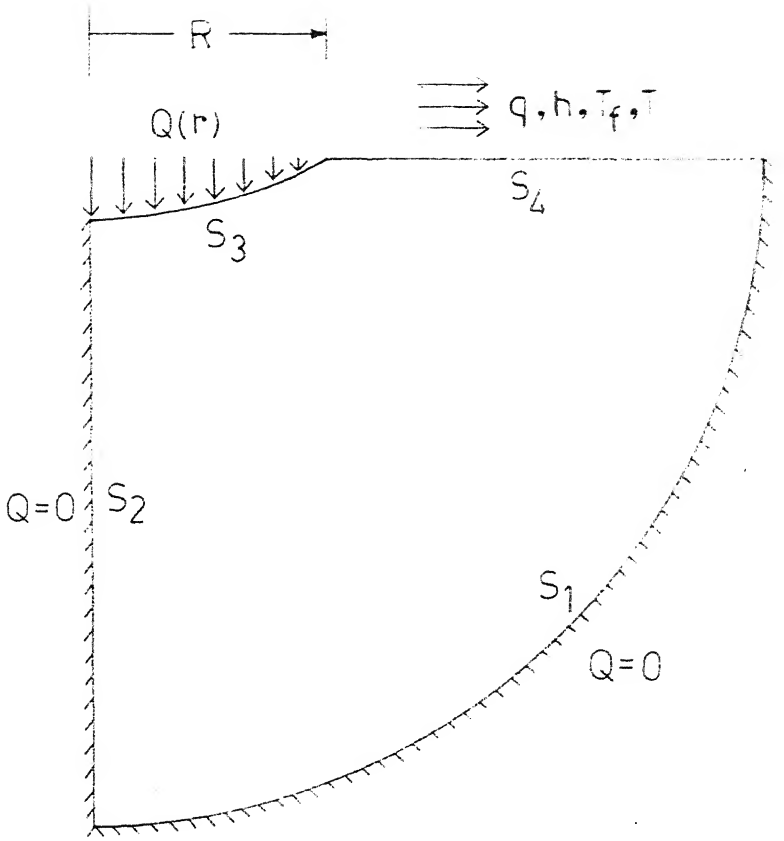

S_1, S_2	Insulated boundary
S_3	Heat flux boundary
S_4	Convective boundary

Fig. 2.4 Boundary conditions on the heat affected zone (HAZ).

The initial condition for temperature for the entire solution domain at the start of the machining operation is assumed to be the room temperature, T_o. Thus

$$T(r,z,o) = T_o \qquad (2.4a)$$

The boundary conditions are :

(i) For all time, the bottom boundary S_1 of the heat affected zone is considered to be insulated in view of the spark being surrounded by neighbouring sparks. Therefore,

$$\frac{\partial T}{\partial n} = 0 \quad \text{on } S_1 \qquad (2.4b)$$

where n is the coordinate normal to S_1.

(ii) Since the heating process is taken as axi-symmetric about the spark axis,

$$\frac{\partial T}{\partial r} = 0 \quad \text{at } r = 0 \qquad (2.4c)$$

(iii) On the top surface, heat flux is considered only upto a radius equal to that of the spark radius, R(surface S_3). For the rest of the portion (Surface S_4), convective heat loss to the dielectric is assumed.

$$\begin{aligned} -k \frac{\partial T}{\partial z} &= h\,(T-T_f) \quad \text{if } r > R \\ &= Q(r) \quad \text{if } r \leq R \end{aligned} \qquad (2.4d)$$

where h is the heat transfer coefficient between the work surface and the dielectric and Q(r) is the heat flux due to the spark.

2.4 CALCULATION OF THE HEAT FLUX DUE TO SPARK :

It is necessary to prescribe the distribution of energy intensity across the spark for the heat transfer model described above, while solving for the temperature in the heat affected zone. Many researchers have considered the spark energy to be uniformly distributed across the spark for mathematical modelling. However, this may not correspond to the actual case since the spark intensity depends on the surface irregularities (surface roughness). Even for a visibly smooth surface, some surface roughness will prevail which has a predominent effect since the spark itself has dimensions of the order of microns. Apart from determining the variation of energy intensity across the spark, it is also necessary to relate the overall parameters of the EDM process to the total power of a spark. This power per spark can be calculated as

$$P_s = \frac{VI \cos\phi}{N} \qquad (2.5)$$

where V is the average voltage, I is the average current, cos ϕ is the duty factor and N is the number of sparks. It is also possible to derive this quantity by integrating the instantaneous discharge power over the pulse time.

Thus,

$$P_s = \frac{E_T}{N} = \frac{1}{N} \frac{1}{t_d} \int_0^{t_d} q(t)\, dt \qquad (2.6)$$

where E_T is the total energy supplied per pulse, t_d is the discharge time and $q(t)$ is the instantaneous power.

In the present work, a Gaussian distribution (Fig.2.5) of the energy intensity is considered within the spark. If q_o is the maximum intensity at the axis of the spark and R is the spark radius, for the Gaussian distribution, we get,

$$q(r) = q_o \exp \left\{ - 2\left(\frac{r}{R}\right)^2 \right\} \qquad (2.7)$$

In terms of the total power per spark, the above expression may be rewritten as

$$q(r) = \frac{2Q}{\pi R^2} \exp \left\{ - 2 \left(\frac{r}{R}\right)^2 \right\} \qquad (2.8)$$

2.5 SOLUTION APPROACH TO THE SPARK EROSION PROCESS :

Earlier authors [1,2,3,4,5,6] have applied the mathematical solutions for the heat conduction problem in cylindrical geometry for both single and multiple spark models. These solutions have a major disadvantage that they consider the heat sources to be placed at the level of the unmachined surface for all times and do not consider the change in geometry after partial machining. The final analytical solution for a single heat source situation is provided in the form of an infinite series given by(See Ref.8)

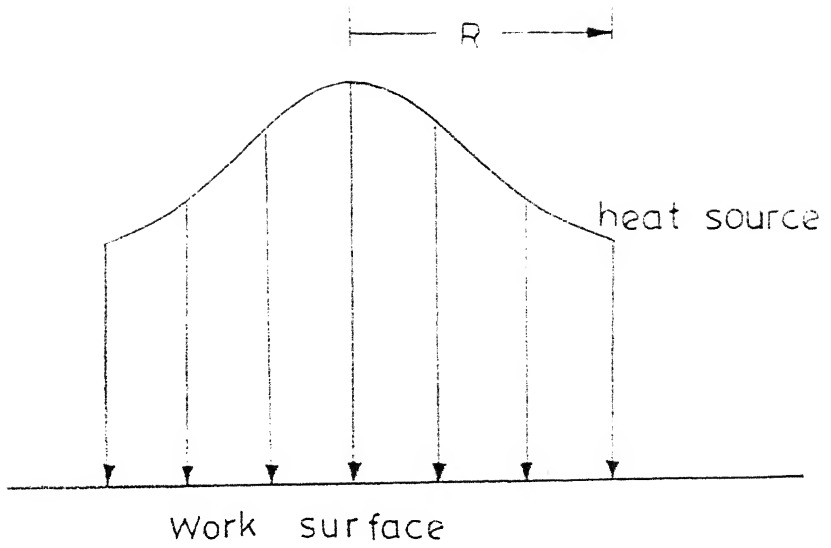

Fig. 2.5 Gaussian distribution of heat source

$$T(r,z,t) - T_o = \sum_{n=1}^{\infty} \frac{C_n}{2\lambda_n} J_o(\lambda_n r) \left[e^{\lambda_n z} \left\{ \operatorname{erf}\left(\lambda_n \sqrt{at} + \frac{z}{2\sqrt{at}}\right) - 1 \right\} + e^{-\lambda_n z} \left\{ \operatorname{erf}\left(\lambda_n \sqrt{at} - \frac{z}{2\sqrt{at}}\right) + 1 \right\} \right]$$

(2.9)

A similar analytical solution can be obtained for a multispark situation also. The rate of machining in these models is predicted by plotting the melting isotherm as a function of time.

In this work, the finite element approach has been applied to obtain more accurate predictions for MRR than the ones available at present. The major contribution of the work is the consideration of the change in shape of the work-surface after partial machining. After each computational machining cycle (which coincides with the time step used), the work surface is updated to the predicted shape of the melting isotherm of that time step. The entire finite element mesh is formulated and these calculations are carried out upto the desired total machining time. The details of the FEM calculations are presented in the next chapter.

2.6 LIMITATIONS OF THE PRESENT MODEL :

1. In actual practice, the EDM cycle consists of OFF time and ON (pulse) time. But in the present model the cycle is having only ON time thereby making it a continuous material removal process.

2. The EDM, working cycle times are of the order of about 100μ seconds. If it is to be taken into account, enormous computational time would be required to obtain machining for about a minute or so. In order to reduce the computer time, larger cycle times are taken.

3. Heat supplied to the evaporation of work material and dielectric are not considered.

4. A prescribed number of sparks (twenty in all calculations), are assumed to strike between the interelectrode gap. In reality, this should be a function of surface roughness and various other factors.

CHAPTER-III

SOLUTION PROCEDURE BY FINITE ELEMENT METHOD

3.1 INTRODUCTION :

The Finite Element Method (FEM) is one of the numerical techniques for obtaining approximate solutions to a wide range of engineering problems. The FE method is widely used to solve a set of partial differential equations because it possesses certain advantages over the other numerical methods. For instance, if we compare the method with finite difference technique, the latter has the disadvantages such as - inaccuracy in approximating, the derivatives of the unknown variable and difficulty in handling complex and irregular geometrics. General purpose software can be developed for FEM problems for a varied range of engineering and mathematical applications with different boundary conditions. Due to the above mentioned reasons, the present study is being treated by FEM technique for solving the heat transfer equations.

In the Finite Element Method, the solution domain is conveniently divided into a finite, small interconnected sub-regions called elements. Solutions are formulated for each element individually and then assembled to form the solution of the entire problem. Since, we have choice over

the shape and grouping of elements, highly complex geometrical shapes can be dealt with. In FEM, the boundary contributions do not appear into the equations for the individual elements and the field variables need not be changed when the boundary conditions are changed. Also, a good approximation to the boundary shape can be obtained due to the great flexibility in choosing the shape of the elements. Complicated material property variations can be incorporated into the system with ease. The systematic procedure for the derivation of the weighting functions makes it a powerful tool for dealing with non-linear and time-dependent field variables.

3.2 DESCRIPTION OF THE FEM PROCEDURE :

The first step in FEM formulation is the conversion of the set of governing equations into an equivalent system of integral equations. Then the solution domain is divided into several small elements of chosen shape and size. The unknown field variables are expressed interms of assumed interpolation functions and the values of the field variables at specified points called nodes with each element. For the finite element representation of a problem, the nodal values of the field variables become the new unknowns. The integral governing equations of the problem are evaluated within each element using the interpolation functions for the element.

All such elemental integrals are assembled to obtain the final matrix equations. The unknown nodal variables can be calculated by solving the assembled matrix equations for the entire solution domain.

Of the procedures available for converting the governing partial differential equations into equivalent integral equations, the most popular ones are the variational procedure and the Galerkin's method. The variational approach relies on the extremization of a functional or a set of functionals, subject to the given boundary conditions. However, functionals may not exist for the problem at hand and the variational approach can not be applied to such problems. The Galerkin's method or method of weighted residuals is more versatile in the sense that it can be extended even to highly non-linear problems where no functional is available. In the present study the Galerkin's approach is used because of its general applicability.

3.3 GALERKIN METHOD :

The Galerkin technique is one among the class of techniques collectively known as the Method of Weighted Residuals. In this approach, the governing differential equations are converted to integral form by minimizing the residue which arises due to the approximate solution.

Two basic steps are involved in the application of the method of weighted residuals. The first step is to assume the general functional behaviour of the dependent field variable in some way so as to approximately satisfy the given differential equation and boundary conditions. Substitution of this approximation into the original differential equation and boundary conditions then results in some error at all locations which is known as the residual. This residual is required to vanish in some average sense over the entire solution domain.

The second step in the method of weighted residuals is to solve the equations resulting from the first step and thereby specialize the general functional form to a particular function, which then becomes the approximate solution sought.

Consider,

$$\mathcal{L}(\phi) = 0 \qquad (3.1)$$

where ϕ is the exact solution to the differential equation. An approximate solution ϕ^* will leave behind a residue, R, such that

$$\mathcal{L}(\phi^*) = R \qquad (3.2)$$

In Galerkin's method, the residue weighted appropriately by suitable weighting function, is minimized over

the whole solution domain D in an integral sense. In mathematical form, this will yield :

$$\int_D W_i \, R \, dv = \int_D W_i \, \mathcal{L}(\phi^*) \, dv = 0 \qquad (3.3)$$

$$\text{for each } i = 1,2,.....m$$

where W_i are the weighting functions. The approximation ϕ^* may be written as a piecewise continuous profile for each element through the expression.

$$\phi^{*(e)} = \sum_{i=1}^{m} N_i^{(e)} \quad \phi_i^{(e)} \qquad (3.4)$$

where m is the number of nodes per element, $N_i^{(e)}$ are the interpolation functions or shape functions and $\phi_i^{(e)}$ are the nodal values of ϕ within the element (e). In Galerkin's procedure, the weighting functions W_i are chosen to be the same as the interpolation function $N_i^{(e)}$ of each element.

It is often advantageous to apply integration by parts to the residue minimization equation (3.3). By this technique, expressions containing lower-order derivatives are obtained which facilitate the use of approximating functions with lower-order inter-element continuity. Another advantage of integration by parts is that this offers a convenient way to introduce the natural boundary conditions of the problem.

3.4 APPLICATION OF FEM PROCEDURE TO THERMAL EROSION IN EDM:

3.4.1 Solution of two-dimensional heat conduction equation:

Consider the heat conduction equation in rectangular geometry

$$\rho C_p \frac{\partial T}{\partial t} = K \left(\frac{\partial^2 T}{\partial x^2} + \frac{\partial^2 T}{\partial y^2}\right) \qquad (3.5)$$

For the approximate temperature solution, the residue of equation (3.5) is

$$\rho\, C_p \frac{\partial T}{\partial t} - K \left(\frac{\partial T}{\partial x^2} + \frac{\partial^2 T}{\partial y^2}\right) = R \qquad (3.6)$$

The weighted residue minimization equations can now be set up as

$$\int\int W_i \left\{\rho\, C_p \frac{\partial T}{\partial t} - K \left(\frac{\partial^2 T}{\partial x^2} + \frac{\partial^2 T}{\partial y^2}\right)\right\} dx\, dy = 0 \qquad (3.7)$$

$$i = 1, \ldots . n$$

where n is the total number of unknowns in the problem. The temperature in equation (3.7) can be expanded in terms of its nodal values and the interpolation functions in the form

$$T = \sum_{j=1}^{n} N_j\, T_j \qquad (3.8)$$

where N_j are the interpolation functions. In Galerkin's method, the weighting functions W_i of equation (3.7) are taken to be the same as the interpolation functions. Therefore,

$$\int\int N_i \left\{ \rho C_p \frac{\partial T}{\partial t} - K\left(\frac{\partial^2 T}{\partial x^2} + \frac{\partial^2 T}{\partial y^2}\right) \right\} dx\, dy = 0 \tag{3.9}$$

Substituting equation (3.8) in equation (3.9) and applying integration by parts,

$$\left[K \int\int \left(\frac{\partial N_i}{\partial x}\frac{\partial N_j}{\partial x} + \frac{\partial N_i}{\partial y}\frac{\partial N_j}{\partial y}\right) dx\, dy \right] \left[T_j \right]$$

$$- \left[\oint N_i K \frac{\partial T}{\partial n} dl \right] + \left[\rho C_p \int\int N_i N_j \, dx\, dy \right] \left[\dot{T}_j \right] = \left[0 \right] \tag{3.10}$$

where the quantities enclosed within the square brackets indicate matrices. The closed boundary integral term of equation (3.10) can be substituted in terms of the boundary conditions of the problem noting that

$$-K \frac{\partial T}{\partial x} = q \quad \text{on heat flux boundary} \tag{3.11a}$$

$$= h(T - T_f) \quad \text{on convection boundary} \tag{3.11b}$$

Now, substituting equations (3.11) into equation (3.10) the following equation is obtained

$$K \sum_{e=1}^{E} \left[\iint_{(e)} \left\{ \frac{\partial N_i}{\partial x} \frac{\partial N_j}{\partial x} + \frac{\partial N_i}{\partial y} \frac{\partial N_j}{\partial y} \right\} dx\, dy \right] \left[T_j^{(e)} \right]$$

$$+ \sum_{e=1}^{Eq} \oint_{(e)} N_i q\, dl + \sum_{e=1}^{Eh} \oint N_i\, h\, (N_j T_j)\, dl$$

$$- \sum_{e=1}^{Eh} \oint_{(e)} N_i\, h\, T_f\, dl + \sum_{e=1}^{E} \left[\rho\, C_p \iint_{(e)} N_i N_j\, dx\, dy \right] \left[\dot{T}_j \right]$$

$$= [\,0\,] \qquad (3.12)$$

where,

E = Number of internal or area elements

Eq = Number of applied heat flux line elements

Eh = Number of convective line elements.

Rewriting the set of equation (3.12),

$$\sum_{e=1}^{E} K^{(e)} \left\{ T^{(e)} \right\} + \sum_{e=1}^{E} q \left[Q_B^{(e)} \right] + \sum_{e=1}^{E_h} \left\{ \left[H_1^{(e)} \right] \left\{ T^{(e)} \right\} - \left[H_2^{(e)} \right] \right\}$$

$$+ \sum_{e=1}^{E} \left[M^{(e)} \right] \left\{ \dot{T} \right\} = [\,0\,] \qquad (3.13)$$

where,

$$\left[K^{(e)} \right] = \iint_{(e)} \left\{ \frac{\partial N_i}{\partial x} \frac{\partial N_j}{\partial x} + \frac{\partial N_i}{\partial y} \frac{\partial N_j}{\partial y} \right\} dx\, dy$$

= Elemental conductivity matrix.

$$[Q_B^{(e)}] = \int_{(e)} N_i \, q \, dl$$

= Applied heat flux boundary vector.

$$[H_1^{(e)}] = \int_{(e)} h \, N_i \, N_j \, dl$$

= Left hand side matrix contribution from a convection boundary element

$$[H_2^{(e)}] = \int_{(e)} h \, T_f \, N_i \, dl$$

= Right hand side vector contribution from a convection boundary element.

$$[M^{(e)}] = \iint_{(e)} N_i N_j \, dx \, dy$$

= Elemental mass matrix.

In the present study, the elements used are eight noded isoparametric elements as shown in Fig. (3.1) whose boundaries are defined by parabolic curves in general. Since, the element sides can assume a curvilinear shape, complex boundaries of the solution domain can be accurately represented. Also, it is possible to define local coordinates ξ and η for an isoparametric element such that the global coordinates x,y of a point inside the element can be expressed in terms of the nodal coordinates and interpolation functions in a similar way as the temperature in equation (3.8). Therefore,

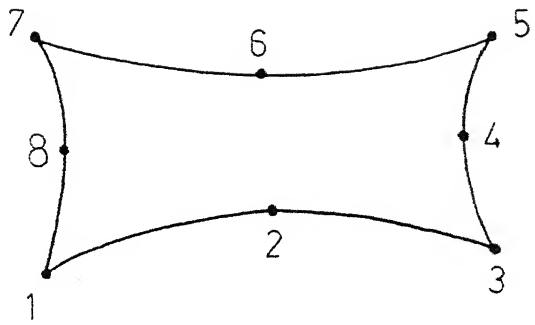

Fig. 3.1 Eight-noded isoparametric element

$$x = \sum_{i=1}^{8} N_i \, x_i \qquad (3.14a)$$

$$y = \sum_{i=1}^{8} N_i \, y_i \qquad (3.14b)$$

The interpolation functions N_i for the 8-noded isoparametric element in terms of the local coordinates ξ and η, are given by the following relations, see ref. [9].

For corner nodes :

$$N_i = \frac{1}{4}(1+\xi_i\xi)(1+\eta_i\eta)(\xi_i\xi + \eta_i\eta - 1) \qquad (3.15)$$

For mid-side nodes:

$$N_i = \frac{1}{2}(1-\xi^2)(1+\eta_i\eta), \text{ if } \xi_i = 0 \qquad (3.16a)$$

$$N_i = \frac{1}{2}(1+\xi_i\xi)(1-\eta^2), \text{ if } \eta_i = 0 \qquad (3.16b)$$

Using the interpolation functions of (3.16) in the finite element equations (3.13), one obtains the global matrices of the form :

$$[M]\{\dot{T}\} + \{[K]+[H_1]\}\{T\} = \{[H_2] - [Q_B]\} \qquad (3.17)$$

where,

[M] is the Global mass matrix.

[K] is the Global conductivity matrix.

$\{\dot{T}\}$ is the vector containing time derivatives of the unknown nodal variable T.

$\{T\}$ is the vector containing unknown nodal variables of temperature.

Equation (3.17) represents a set of ordinary differential equations of the variable T and its time derivatives. These sets of equations are solved by applying the finite difference technique.

The steps involved are as follows :

For k^{th} time step equation (3.17) may be written as

$$[M]\{\dot{T}\}^{k} + \{[K] + [H_1]\}\{T\}^{k} = \{[H_2] - [Q_B]\}^{k} \quad (3.18)$$

For the $(k+1)^{th}$ time step, it is :

$$[M]\{\dot{T}\}^{k+1} + \{[K] + [H_1]\}\{T\}^{k+1} = \{[H_2] - [Q_B]\}^{k+1} \quad (3.19)$$

The finite difference scheme for the time derivative can now be written in a most general form as

$$\{T\}^{k+1} - \theta \Delta t \{\dot{T}\}^{k+1} = \{T\}^{k} + (1-\theta)\ \Delta t \{\dot{T}\}^{k} \quad (3.20)$$

where,

Δt is the required time step.

k and k+1 refer to the k^{th} and $k+1^{th}$ time level.

θ is a constant, which decides the particular type of the scheme to be chosen.

$\theta = 0$ gives the Explicit or Forward difference scheme.

$\theta = 0.5$ gives the Crank-Nicholson or Mid-difference scheme.

$\theta = 1.0$ gives the Implicit or Backward difference scheme.

In the present case, the implicit scheme is employed. The implicit method uses the time derivative evaluated at the $(k+1)^{th}$ time level. Therefore, for each increment of time by Δt, the calculation of the nodal temperatures at the new time level requires the solution of a set of simultaneous algebraic equations. The solution is thus marched in time, in steps of Δt until the desired final time is reached. Although computations involving the implicit method are more complicated than that of the explicit method, the implicit formulation has the important advantage of being unconditionally stable [10]. Larger values of Δt may therefore be used resulting in less computational time. Substituting equation (3.20) into equations (3.18) and (3.19) and rearranging, we get,

$$\left([M] + \theta \Delta t \left\{ [K] + [H_1] \right\} \right) \{T\}^{k+1}$$

$$= \left([M] - (1-\theta) \Delta t \left\{ [K] + [H_1] \right\} \right) \{T\}^{k}$$

$$+ \Delta t \left\{ [H_2] - [Q_B] \right\} \qquad (3.21)$$

Since the vector $\{T\}^k$ is known for each k^{th} time, the nodal temperature vector $\{T\}^{k+1}$ can be calculated.

3.5 CONVERSION OF THE PROBLEM TO AXI-SYMMETRIC FORMULATION:

In order to convert the problem to an axi-symmetric situation, the following modifications are carried out in the governing differential equation (3.5).

Galerkin residue equation are :

$$\int\int N_i \left(\nabla^2 T - \frac{\partial T}{\partial t} \right) dv = [0] \qquad (3.22)$$

where,

dv = volume of a differential control volume under consideration.

= $2\pi x \, dx \, dy$ for the axi-symmetric geometry.

The equation (3.22) can be written as :

$$\int\int N_i \left\{ \left(\nabla^2 T - \frac{\partial T}{\partial t} \right) \right\} 2\pi x \, dx \, dy = [0]$$

or

$$\int\int \left(\underline{\nabla} \cdot (N_i \, \underline{\nabla} T) - \underline{\nabla} N_i \cdot \underline{\nabla} T - \frac{\partial T}{\partial t} N_i \right) 2\pi x \, dx \, dy$$

$$= [0] \qquad (3.23)$$

The first term of equation (3.23) after the application of the divergence theorem, can be written as :

$$\iint \underline{\nabla} \cdot (N_i \underline{\nabla} T)\, dv = \oint \underline{n} \cdot N_i \underline{\nabla} T\, 2\pi x\, dl - \iint \underline{\nabla} N_i \cdot \underline{\nabla} T\, 2\pi x\, dx\, dy$$

Substituting the above expression into the equation (3.23) we get,

$$\left[\iint \left\{ \frac{\partial N_i}{\partial x} \frac{\partial N_j}{\partial x} + \frac{\partial N_i}{\partial y} \frac{\partial N_j}{\partial y} \right\} x\, dx\, dy \right] [T_j] - \left[\iint N_i N_j\, x\, dx\, dy \right] [\dot{T}_j] + \oint N_i\, k \frac{\partial T}{\partial x_n}\, x\, dl = [0] \qquad (3.24)$$

The last term in equation (3.24) can be rewritten in terms of the applied boundary conditions of the problem. The resulting equations are of the form:

$$\sum_{e=1}^{E} \left[\iint \left\{ \frac{\partial N_i}{\partial x} \frac{\partial N_j}{\partial x} + \frac{\partial N_i}{\partial y} \frac{\partial N_j}{\partial y} \right\} x\, dx\, dy \right] [T_j^{(e)}] + \sum_{e=1}^{E^q} \int_{(e)} N_i\, q\, x\, dl + \sum_{e=1}^{E^h} \int N_i h\, (N_i T_i)\, x\, dl + \sum_{e=1}^{E} \left[\iint_{(e)} N_i N_j\, x\, dx\, dy \right] [\dot{T}_j] = [0] \qquad (3.25)$$

The set of simultaneous ordinary differential equations represented by (3.25), can be solved using the implicit finite difference procedure as discussed in the previous section.

3.6 PHYSICAL REPRESENTATION OF THE PROBLEM :

In order to proceed with the calculation for material removal, the geometry of the solution domain and the boundary conditions should be well defined. The physical domain, and the node numbering of the problem are done as shown in Fig. 3.2 and 3.3 respectively. The figures are self explanatory.

3.7 DOMAIN VARIATION WITH TIME :

Initially the domain is as shown in Fig. 3.3 and is considered to be at room temperature. After the discharge takes place for a given amount of time, the value of temperature at each node changes, depending on the type of boundary conditions, the domain is subjected to. Since we propose material removal to be primarily due to melting, the shape of the melting isotherm is drawn. A typical melting isotherm has a shape as shown in Fig. 3.4. The material above the isotherm (hatched area) is considered to be removed within the time step considered for computation. Now, for the next discharge, this melting isotherm becomes

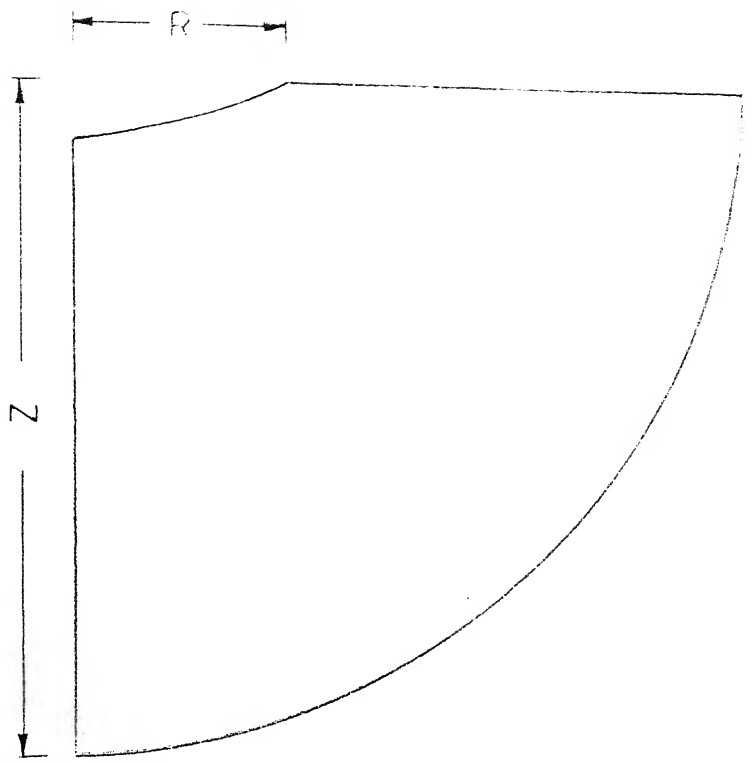

R Radius of spark
Z Depth of penetration

Fig. 3.2 Physical domain (work piece configuration)

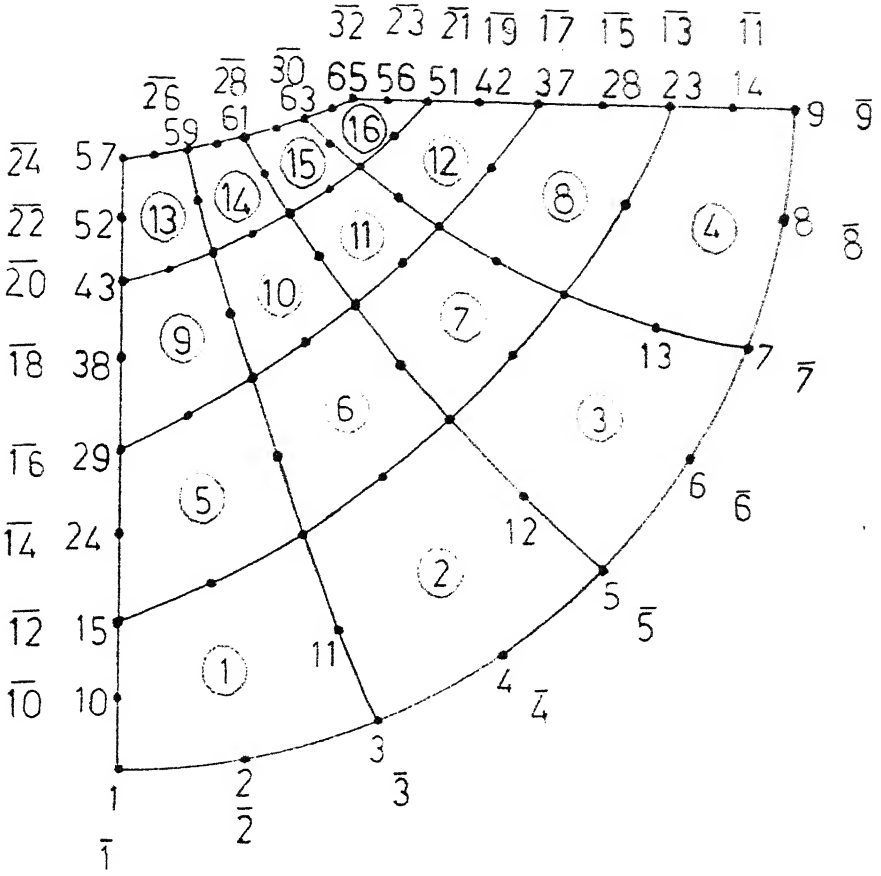

1,2,3 - Node Numbers
(1), (2), (3) - Element Numbers
1̄, 2̄, 3 - Boundary Node Numbers

Fig. 3.3 Numbering of the grid of Fig. 3.2

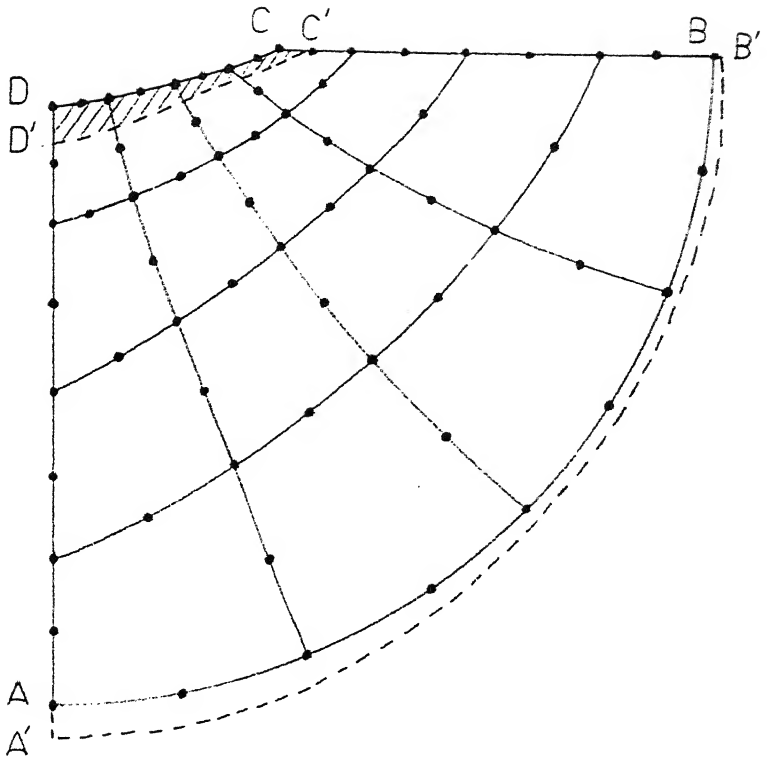

▨	Region above melting temperature or Material removed.
---	Changing surfaces (boundaries)
C′D′	Melting isotherm

Fig. 3.4 Melting isotherm and surface change representation.

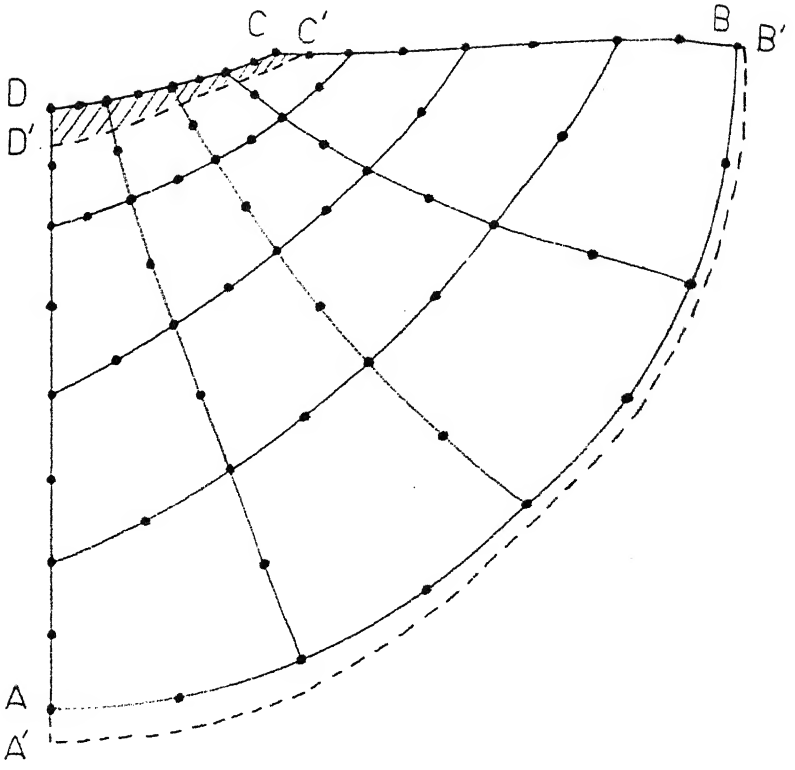

▨	Region above melting temperature or Material removed.
---	Changing surfaces (boundaries)
C′D′	Melting isotherm

Fig. 3.4 Melting isotherm and surface change representation.

the surface of the work piece on which the sparking occurs. The nodes of the bottom surface (AB) are also moved a distance equal to those of the top surface, so that for any discharge the depth and radius of heat affected area for a spark remains relatively large (about 10 times) with respect to the spark radius. This process of updating the domain geometry is done everytime before applying the subsequent discharge. Thus, the FEM analysis is performed for the modified geometry after each time step.

CHAPTER- IV

RESULTS AND DISCUSSIONS :

From the finite element formulation of the EDM process described in the previous chapter, results have been predicted for the temperature variation with respect to time and space in an H.S.S. work piece which is initially at room temperature. Assuming that the regions which attain a temperature above the upper limit of melting temperature ($T_m+\Delta$) are completely removed, the rate of material removal and the shape of the crater in the work piece for a typical spark have also been predicted.

The results corresponding to a single spark have been obtained by considering total machining time of the order of typical pulse time with a very high power input. To get realistic results of an actual EDM problem a multispark model has also been solved considering 20 sparks with a continuous but low power input over a total machining time which is much larger than the pulse time.

In Fig. 4.1 the amount of material removed by a single spark within a pulse time of 600 μs has been compared with the analytical results of Snoeys and Dyck

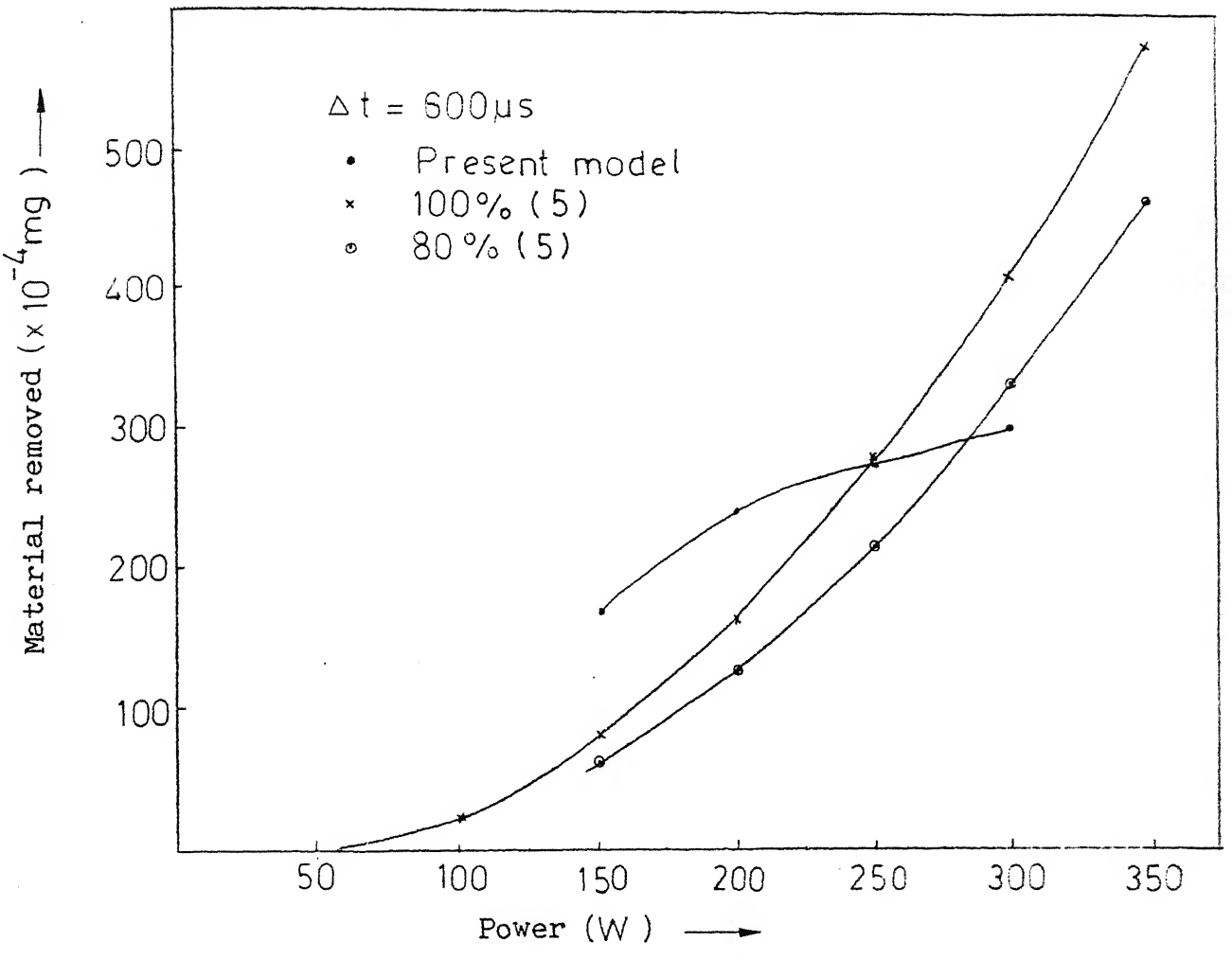

Fig. 4.1 Material removed versus power (a comparison)

as presented in Ref. [5]. Various values of average discharge power during the pulse have been considered for comparison. Since the model presented [Ref. 5] takes into account partial evaporation and partial melting, the appropriate curve that needs to be compared with our result is the 100 %. melting curve. For the range of powers considered, the analytical and numerical results match approximately. The slight discrepancy observed between the results can be explained from the fact that no heat loss from the top surface is considered in the analytical result and also the heat flux is always applied at the top surface. The present formulation on the other hand accounts for heat loss from the top surface into the dielectric medium and also it updates the whole surface shape after each small time step Δt.

The amount of material removed with time has been plotted for three different numerical cycle times in Fig. 4.2a. It is seen from the figure that the amount of material removed increases with time at a non-uniform rate. For certain times the rate of machining is very high and for some others it is very low. This non uniformity in the rate of material removal can be attributed to the processes of temperature rise from room conditions upto the melting value and the phase change from solid to liquid, successively.

With respect to numerical cycle time it is observed that smaller the time step higher the value of material removed. When small time steps are used the molten material is removed more frequently and the newly formed surface is directly exposed to the heat source. This results in a higher overall material removal rate. In Fig. 4.2b the shape of the crater at the end of a total machining time of 2.5 sec. is shown for different numerical cycle times. For the reasons discussed above, the depth of penetration is more, for smaller Δt.

In Fig. 4.3 the change in the shape of the crater with machining time for different time step Δt is presented. It is observed that in the initial stages of machining the crater extends deeper along the centre line of the spark. For later times, it spreads more in the radial direction upto spark radius.. For still larger machining time, the crater develops a taper along the sides. The width of the crater at the top surface of the workpiece is nearly equal to the spark diameter. In the present formulation a Gaussian distribution of heat flux intensity has been assumed within the spark. Due to this the rate of penetration along the centre line of the spark is higher for all times. It is also seen that for a smaller numerical cycle time the crater volume is larger at any instant of time.

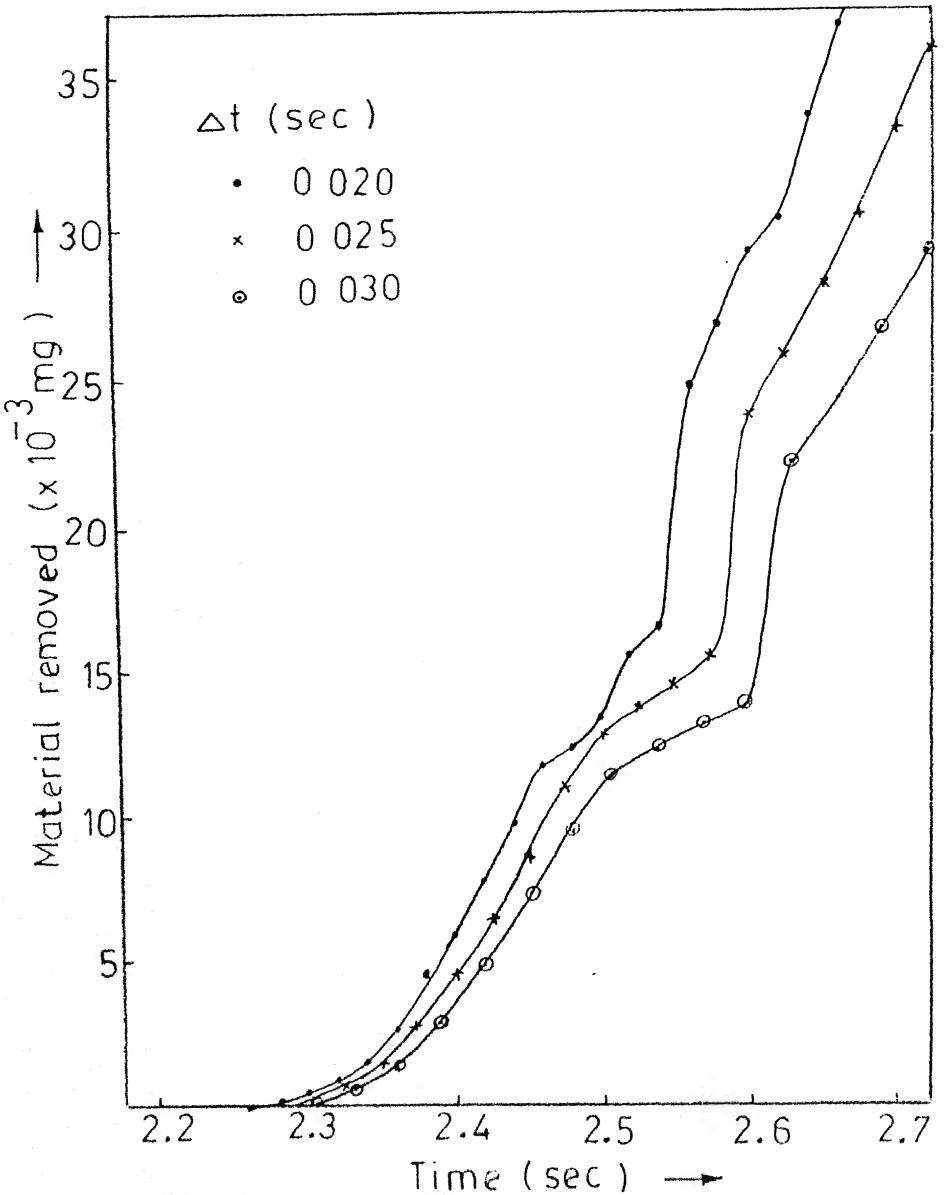

Fig.4.2a Effect of time step Δt on material removal

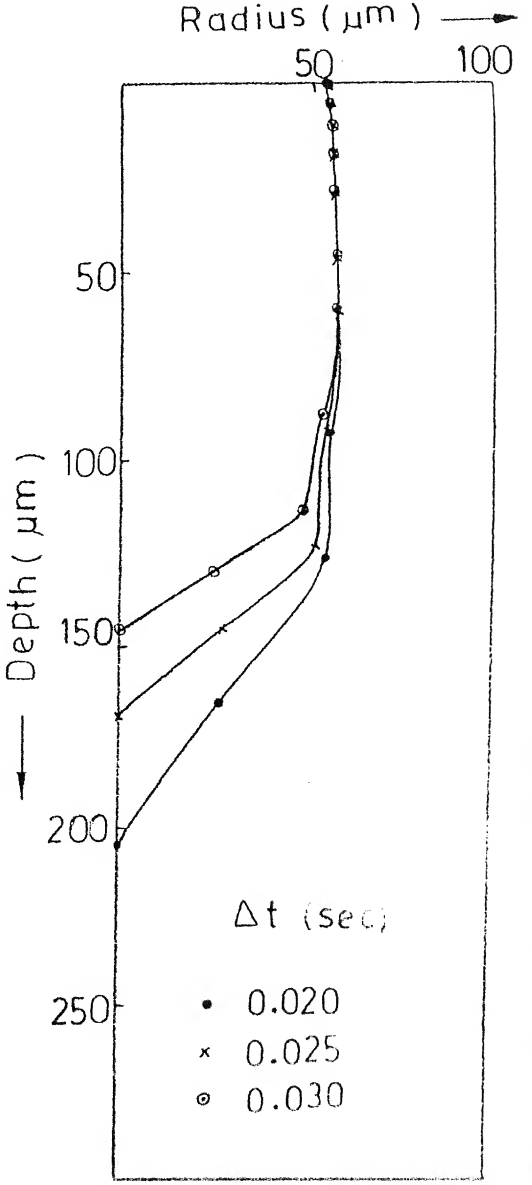

Fig. 4.2b Effect of Δt on crater shape at the end of 2.5 sec of machining

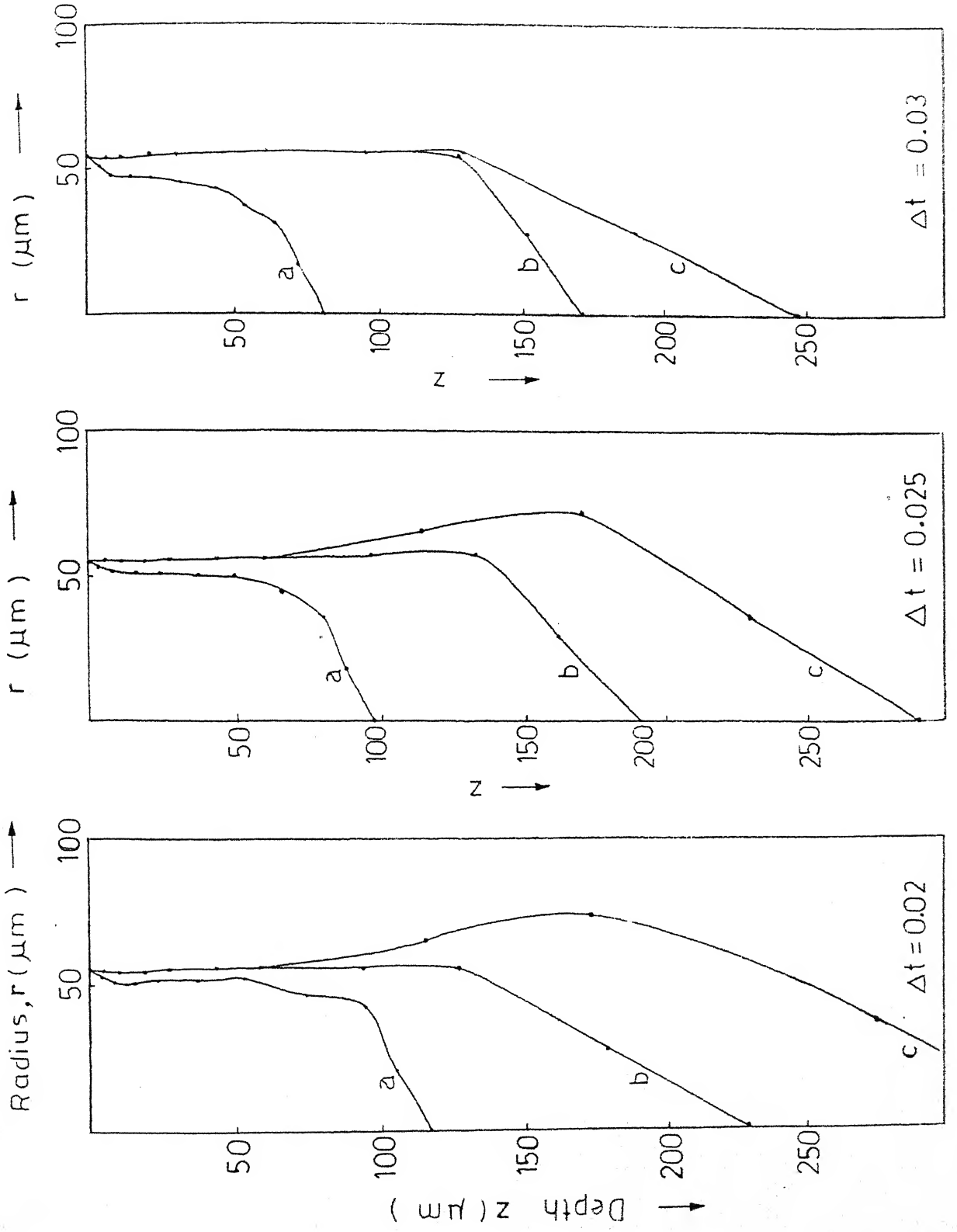

Machining time (sec) a - 2.4 b - 2.5 c - 2.6

Fig. 4.3 Crater formation with different time step

In Fig. 4.4(a and b) the effect of spark radius on material removal is shown. The plots indicate that at a fixed power level, the smaller the spark radius higher is the amount of material removed for a given time. For a smaller spark radius, the power intensity is higher and this leads to a higher rate of material removal. It is also seen that machining starts later if the spark size is larger. In Fig. 4.4b the shape of the crater after a machining time of 2.5 sec. shows that for a smaller sized spark the width of the crater is less but the depth is much more than those of a larger sized spark. Thus it is clear that the radius of crater depends on the radius of spark but the depth of crater after a certain machining time depends on the average power intensity of the spark. These conclusions are further confirmed by the shapes of craters shown in Fig. 4.5 at various instances of time for two different spark radii.

The effects of power per spark upon material removal is shown in Fig. 4.6. The chief influence of increasing the power per spark is that melting starts early. Infact there is an almost constant time gap between all the curves at all times. However, there is a very slight increase in slope with an increase in power per spark so that the material removal is slightly higher. The shapes of the craters at various instances of time, Fig. 4.7 , are shown for different power per spark. The crater shapes confirm the finding discussed above.

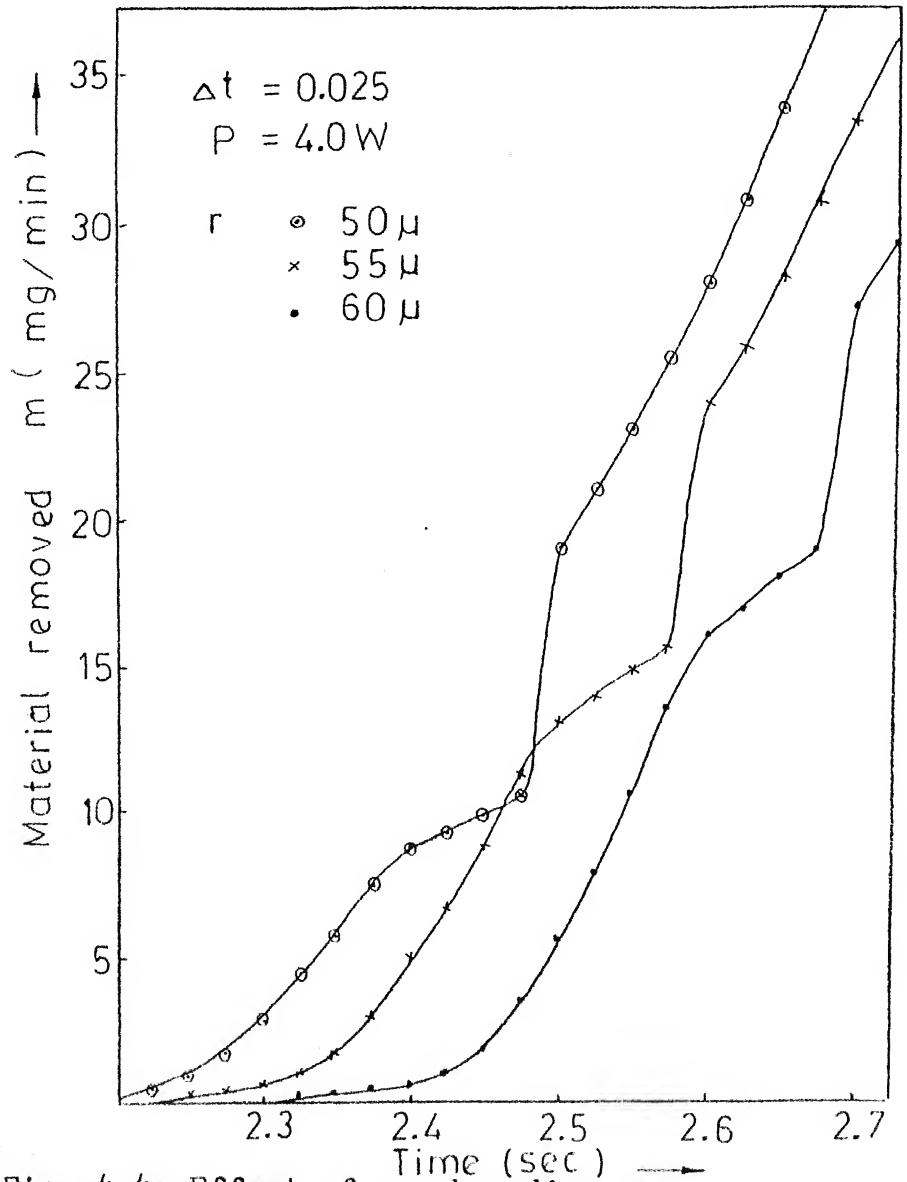

Fig. 4.4a Effect of spark radius on material removal

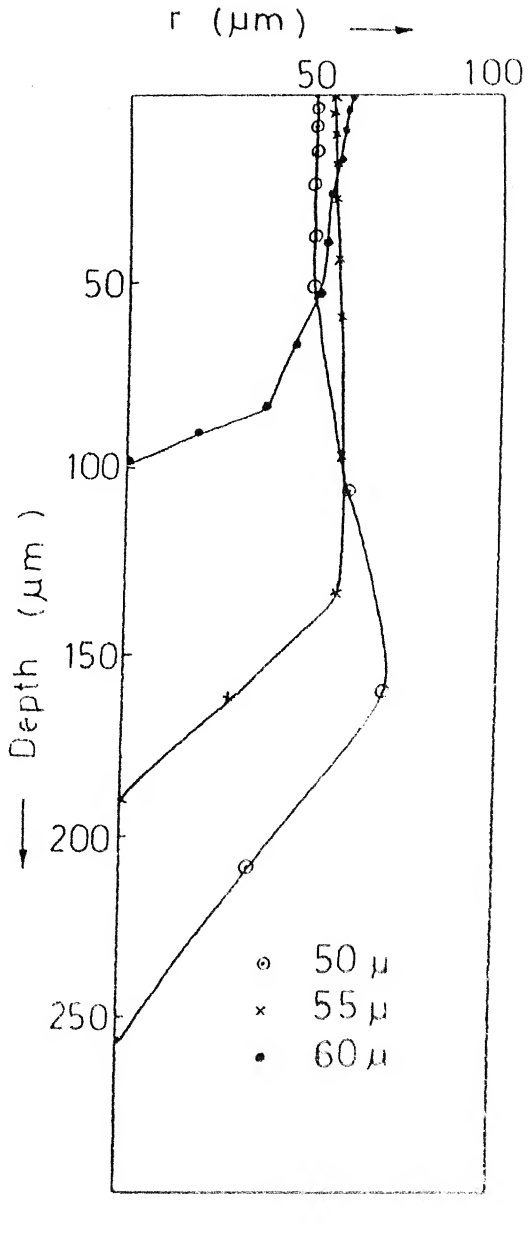

Fig.4.4b Effect of spark radii on crater shape at the end of 2.5 sec of machining

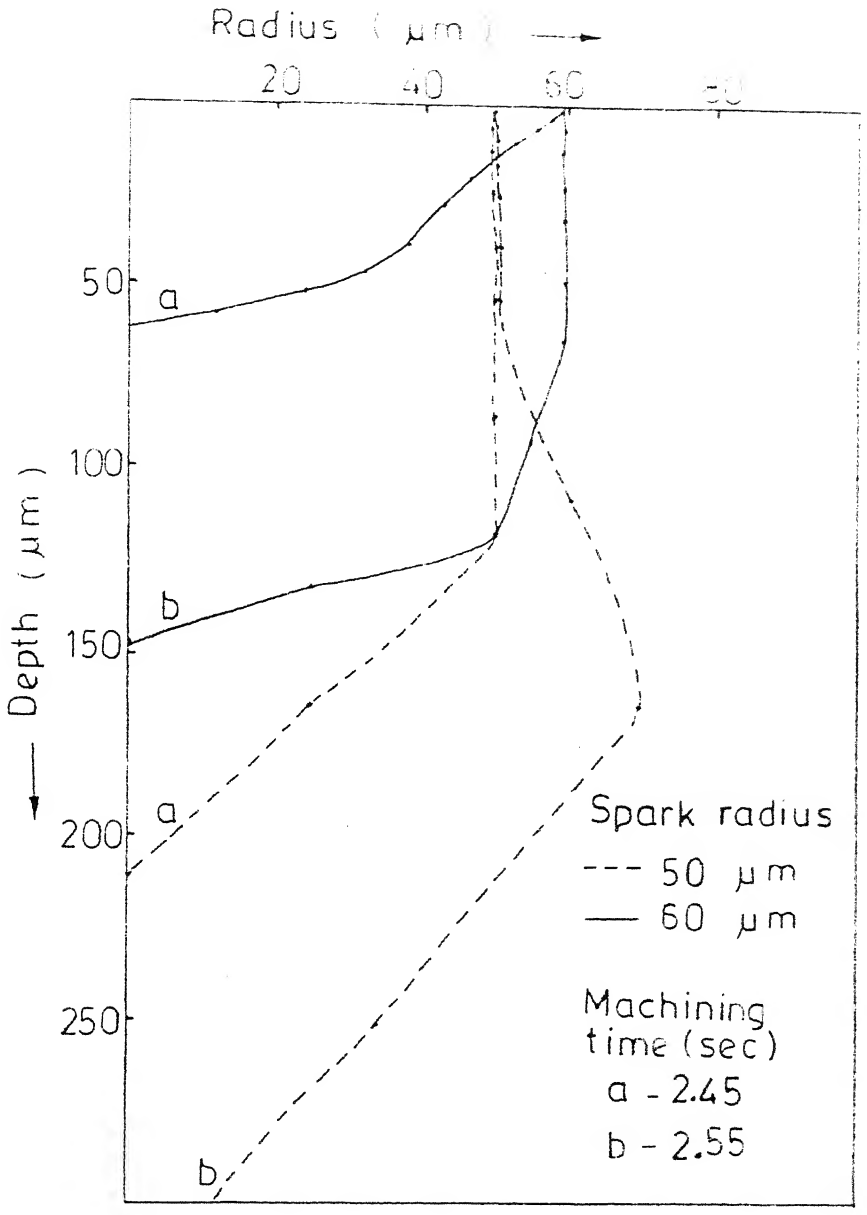

Fig. 4.5 Comparison of crater formation for different spark radii

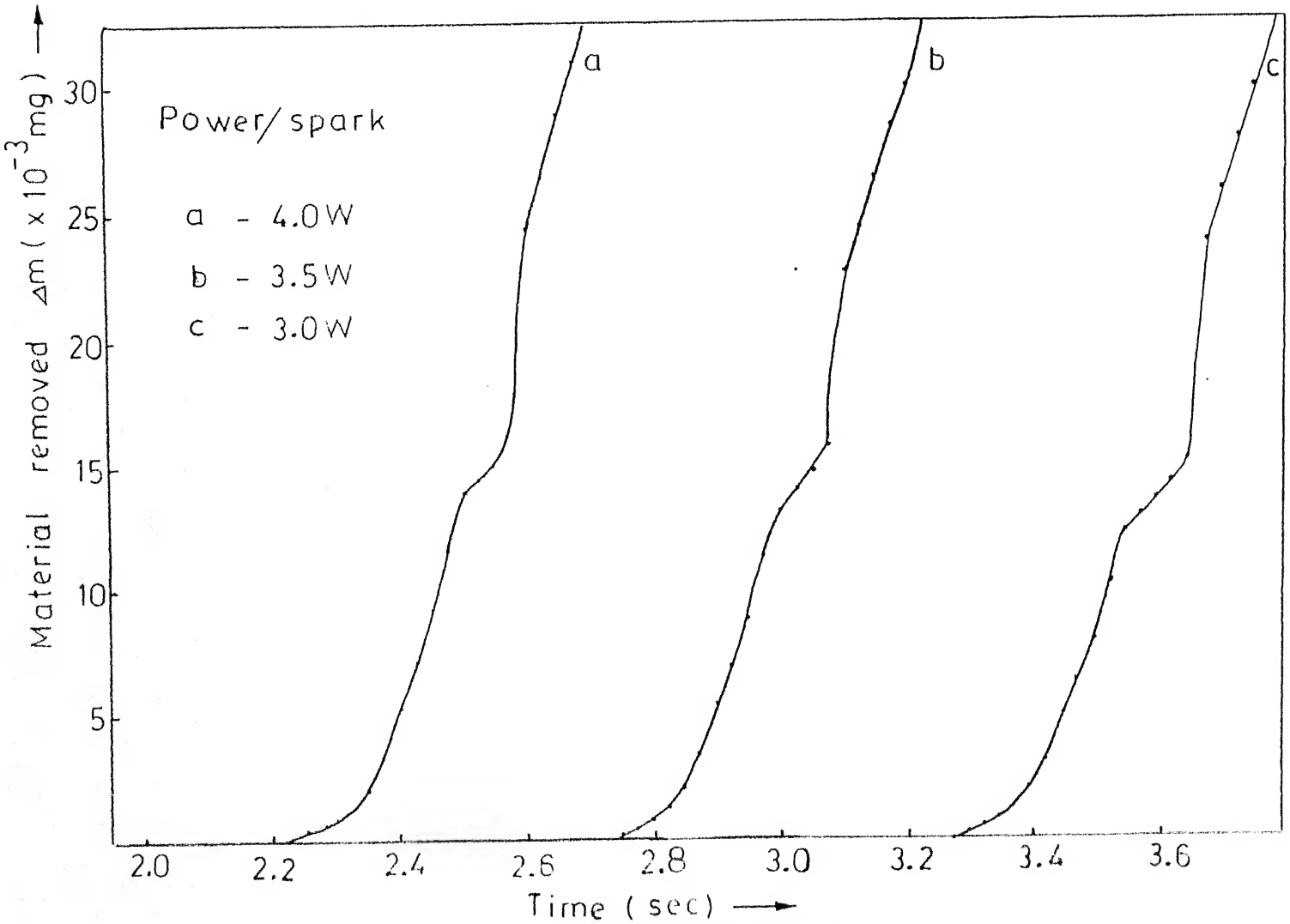

Fig. 4.6 Time variation of material removal with power variation

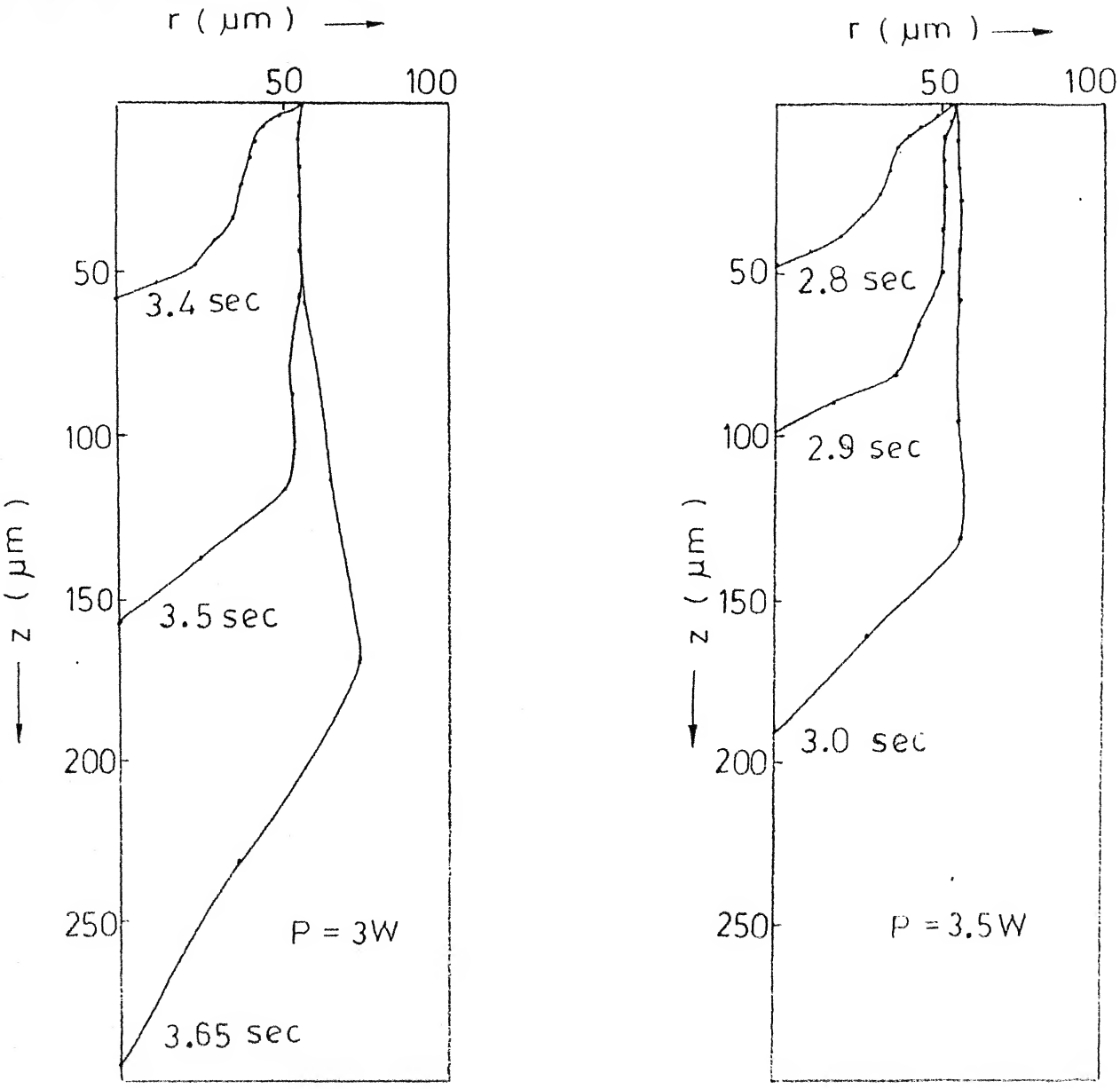

Fig. 4.7 Typical crater shapes for different levels of power per spark

In Fig. 4.8 the variation of material removal rate (MRR) with power per spark has been presented for a given spark radius and numerical cycle time. As expected MRR increases with power, since higher power input can supply more heat for melting the material. The MRR however, has a tendency to level off as power input per spark increases. This may be because of heat losses increasing at a fast rate.

In Fig. 4.9 the effect of cycle time Δt upon MRR has been shown, with other parameters fixed. As cycle time decreases, MRR increases because of direct access of the work surface to the heat input more frequently. The MRR is seen to be very sensitive to changes in the value of the spark radius (Fig. 4.10). As the spark radius decreases the MRR increases very rapidly tending to approach the limit of a point source at small values of radius. Similar trends with variation in spark radius have been reported by Erden and Kaftanaglu [5].

The experimentally observed values of MRR by Indurkhya (11) for three different machining conditions are also shown in the figure. It is seen that the range of variation of MRR is the same as in the present results, further validating our model. More detailed comparison of the experiment of Ref. [11] and present results is not possible due to the inavailability of important numerical parameters such as spark

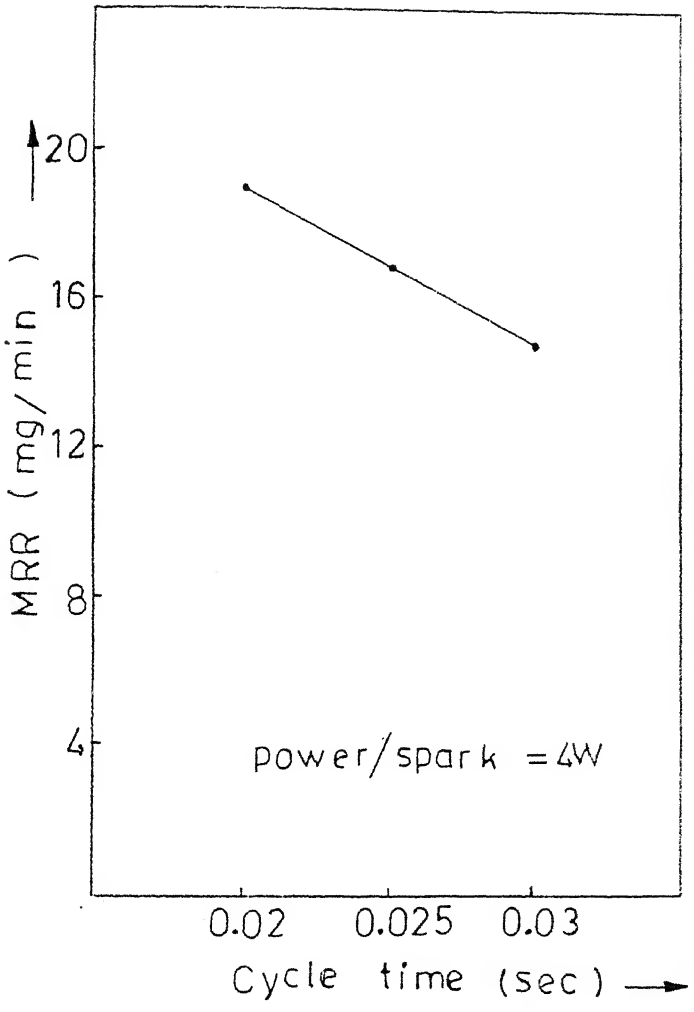

Fig. 4.9 Variation of average MRR with Δt (cycle time)

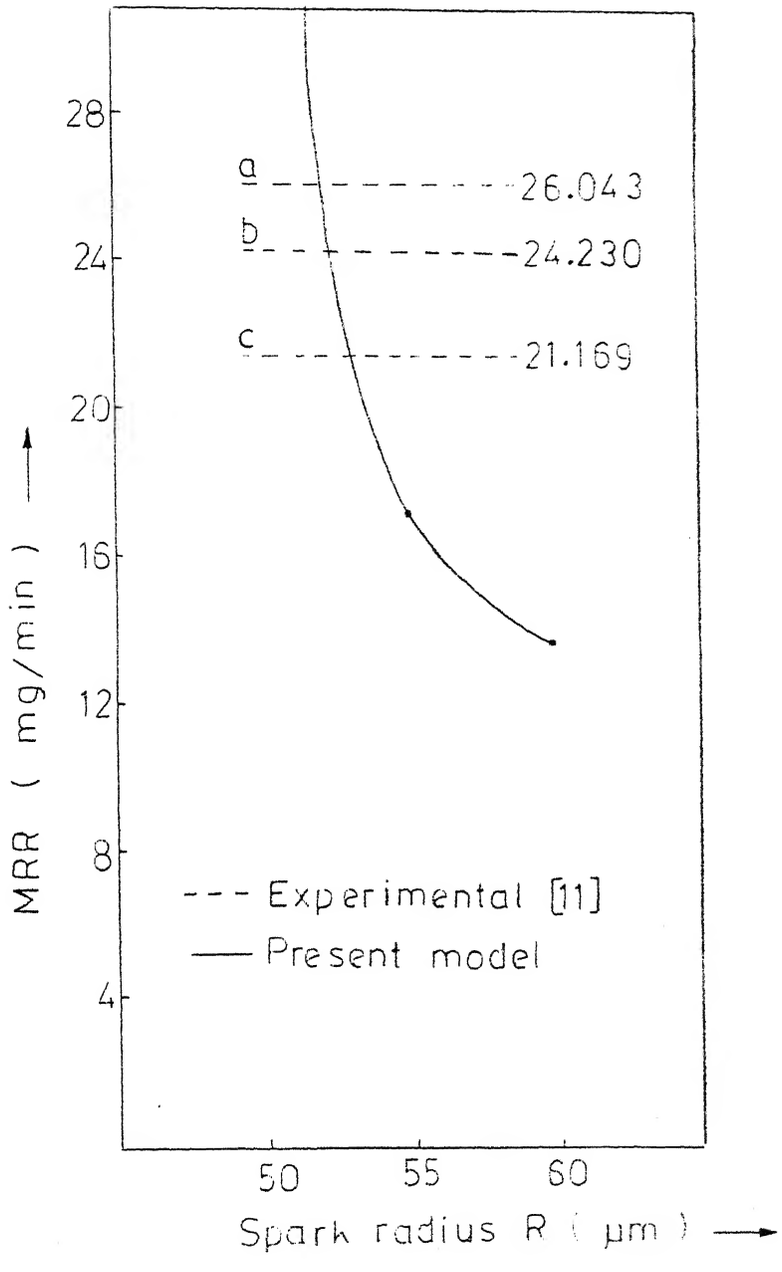

Fig. 4.10 Variation of average MRR with spark radius

radius and number of sparks in the gap for the experimental study. Also our theoretical study has a limitation of the continuous heat flux model which has been invoked to reduce the computational effort. The experimental machining conditions for which MRR values have been taken from Ref. [11] are summarized in Table 4.1

The variation of material removal rate with machining time is shown in Fig. 4.11 for three different numerical cycle times. The MRR rapidly increases in the beginning after actual machining starts and a little while later it reaches a more or less steady value. There are always a few fluctuations in MRR for all time indicating the basic random nature of the EDM process.

Fig. 4.12 gives the isotherms of different temperature values. The plotted values show the movement of (melting) crater and it is fairly clear that the temperature increases very rapidly with depth in the (z) direction when compared to the radial (r) direction.

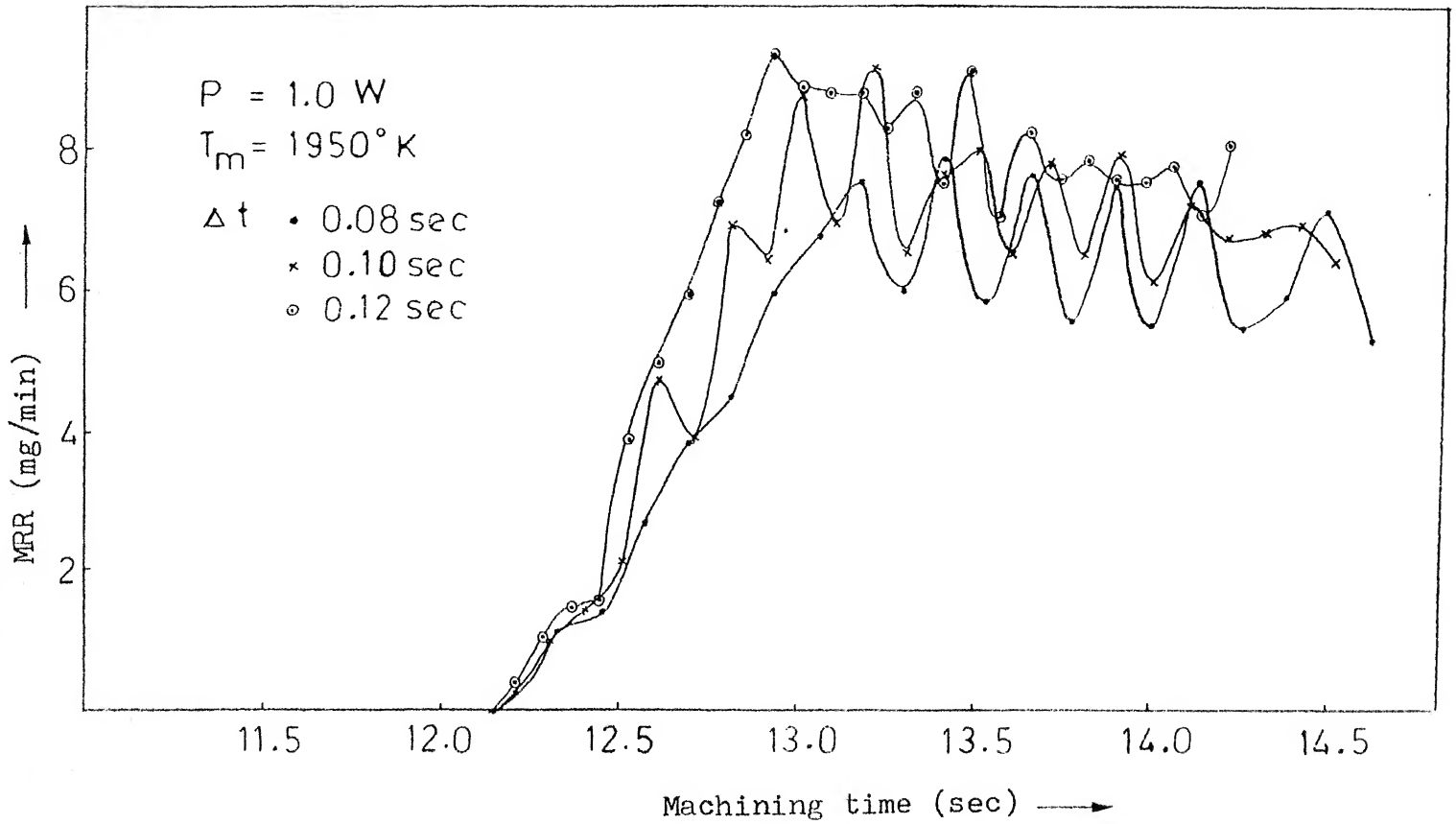

Fig. 4.11 Variation of MRR with machining time for different Δt

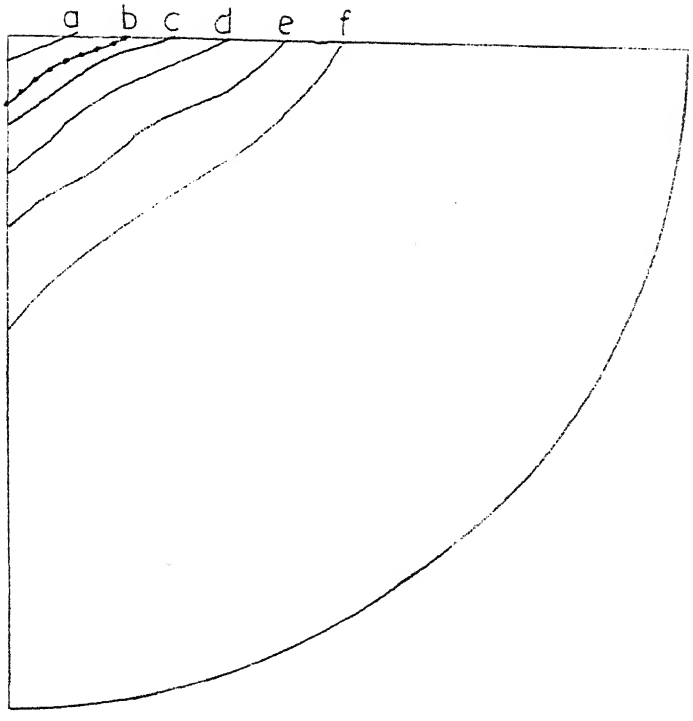

Temperature (K)

a - 2000
b - 1950 ---- Melting
c - 1900
d - 1875
e - 1850
f - 1800

Fig. 4.12 Typical isotherms prevailing in the work piece

Table 1 Experimental MRR values for different machining conditions

Curve	ON time µs	Tool radius mm	M R R mg/min
a	20	5	26.043
b	100	6	24.230
c	100	5	21.169

5. CONCLUSIONS AND SUGGESTIONS

5.1 CONCLUSIONS :

1. The physical formulation and the Finite Element formulation of the EDM process presented in this work appear to describe the actual phenomena reasonably accurately. The present analysis incorporates many improvements over previous theoretical works such as the accounting of the movement of the work surface, accounting of heat losses to the dielectric medium and variation of power intensity within the spark. Both single spark and multispark models have been developed to predict the rate of machining within a single pulse and also over many pulses upto a reasonable machining time.

2. It is observed that the width of the spark depends on spark radius while the depth of penetration depends upon the power intensity.

3. The numerical cycle time (time step, Δt) plays an important role in accurately predicting material removal.

4. The material removal rate increases with power per spark, decreases with an increase in time step Δt.

It has a very strong dependence on spark radius appearing to reach the limit of infinity i.e. for a point source for very small spark radii. With respect to machining time the MRR increases rapidly immediately after the start of machining but soon it reaches a steady state value.

5.2 SUGGESTIONS FOR FUTURE WORK :

1. The effect of evaporation of material can be considered by incorporating latent heat of boiling (evaporation) in addition to the latent heat of melting.

2. The number of sparks can be assumed based on the surface roughness of tool and work piece materials.

3. The heat source location can be assumed to be moving, with respect to time and space based on the relative surface roughness prevailing in the inter electrode gap.

4. The temperature distribution in tool and dielectric medium can be predicted by extending the model to tool surface. Relative electrode wear can also be predicted.

REFERENCES :

1. C.C. Marty, "Investigation of surface temperature in EDM"; Vol. 99, 1977, pp 682-684, Journal of Engineering for Industry.

2. Y. Mukoyama, "The Mechanism of Electro-Discharge Machining", Bulletin of the Japan Soc. of Prec. Engg. , vol. 2, No.4, 1968, pp 288-295.

3. S.T. Jilani, and P.C. Pandey ,"An analysis of surface erosion in Electrical Discharge Machining", Wear vol. 84, 1983, pp. 275-284.

4. S.W. Dharmadhikari, and C.S. Sharma," Determination of material removal in EDM using a multiple heat source model", Proc. of 9th AIMTDR Conf. IIT. Kanpur, Dec. 1980, pp. 316-320.

5. A Erden, and B. Kaftanoghlu, "Heat transfer modelling of Electric Discharge Machining", Proc. of 21stIMTDR Conf. Macmillan, London, 1980, pp 351-358.

6. R. Snoeys and F. Van Dyck, "Investigations of EDM operations by means of thermo-mathematical model", Annals of CIRP, vol. 20 No.1, 1971, pp. 35-36.

7. P.C. Pandey, and H.S. Shan, "Modern Machining Processes", Tata McGraw-Hill, New Delhi, 1980.

8. H.S. Carslaw, and J.C. Jaeger, "Conduction of heat in solids", Clarendon-Oxford Press, Oxford, 1959, pp. 264.

9. C. Taylor , and T.G. Hughes, "Finite Element Programming of the Navier-Stokes Equation", 1st edition, Pineridge press Ltd., Swansea, UK, pp 39, 1981.

10. Frank P. Incropera, and David P. Dewitt, "Fundamentals of Heat and Mass Transfer," 2nd Edition, John Wiley and Sons, New York, pp. 221, 1985.

11. Gopal Indurkhya, "Some Investigation into Electro discharge drilling process", M.Tech. thesis, IIT., Kanpur, May 1985.